UNIVERSITY OF CALIFORNIA SAN DIEGO

Oral Squamous Cell Carcinoma (OSCC) Learn from Tumor Micro-Environment to be Metastatic

A Dissertation submitted in partial satisfaction of the requirements
for the degree Doctor of Philosophy

in

Bioengineering

by

So Youn Moon

Committee in charge:

Professor Adam J. Engler, Chair
Professor Stephanie I. Fraley
Professor Frank B. Furnari
Professor Marcelo L. Lamers
Professor Jing Yang

2024

©

So Youn Moon, 2024

All rights reserved

The Dissertation of So Youn Moon is approved, and it is acceptable in quality and form for publication on microfilm and electronically.

University of California San Diego

2024

TABLE OF CONTENTS

DISSERTATION APPROVAL PAGE iii
TABLE OF CONTENTS iv
LIST OF FIGURES v
LIST OF SUPPLEMENTAL FILES vi
ACKNOWLEDGEMENTS vii
VITA viii
ABSTRACT OF THE DISSERTATION ix
Chapter 1 CELL CONTRACTILITY DRIVES MECHANICAL MEMORY OF ORAL SQUAMOUS CELL CARCINOMA (OSCC) 1
1.1 Introduction 1
1.2 Results 3
1.3 Discussion 12
1.4 Materials and Methods 15
Chapter 2 PARACRINE INTRA-TUMOR CELL SIGNALING ENHANCES TUMOR METASTASIS IN ORAL SQUAMOUS CELL CARCINOMA (OSCC) 23
2.1 Introduction 23
2.2 Results and Discussion 25
2.3 Materials and Methods 37
REFERENCES 44

LIST OF FIGURES

Figure 1.1: Contractility modifies cell behavior in oral squamous carcinoma in vivo and increases EMT marker expression in vitro 4

Figure 1.2: Stiffness-induced changes in E-Cadherin localization and NMM2 expression are durable in tissue adjacent epithelium-like stiffness. 6

Figure 1.3: Acquisition of mechanical memory in 2D and 3D environment is affected by contractility. 7

Figure 1.4: Mechanical memory involves AKT and FAK signaling 9

Figure 1.5: Transcriptomic differences between “Learn” vs. “Don’t Learn/Forget” groups. 11

Figure 2.1: Motility change in Cal27 after indirect co-culturing with SCC25 using conditioned media (CM). 26

Figure 2.2: Transcriptomic change in Cal27 after being cultured with SCC25-CM for 3 days.... 28

Figure 2.3: Cytokines involved in metastasis-inducing paracrine cell signaling 32

Figure 2.4: Patient survival rate with respect to the transcriptomic expression of the cytokines of interest..... 33

Figure 2.5: MAPK and AKT signaling pathways activated in response to paracrine cell signaling 36

LIST OF SUPPLEMENTAL FILES

Moon_Supplemental Figures and Supplemental Table Caption.pdf

Moon_Supplemental Table 1.xlsx

Moon_Supplemental Table 2.xlsx

Moon_Supplemental Table 3.xlsx

Moon_Supplemental Table 4.xlsx

Moon_Supplemental Table 5.xlsx

Moon_Supplemental Table 6.xlsx

Moon_Supplemental Table 7.xlsx

ACKNOWLEDGEMENTS

I would like to acknowledge Professor Adam J. Engler for his support as the chair of my committee. His guidance and support through this journey are invaluable.

Chapter 1, in full, is a reprint of the material as it appears in Cell Contractility Drives Mechanical Memory of Oral Squamous Cell Carcinoma. Moon, So Youn; Campos, Paloma S.; Matte, Bibiana F.; Placone, Jesse K.; Zanella, Virgi L. G.; Martins, Manoela D.; Lamers, Marcelo L.; Engler, Adam J., Molecular Biology of the Cell, 2023. The dissertation author was the primary investigator and author of this paper.

Chapter 2, in full, is currently being prepared for submission for publication of the material. Moon, So Youn; Lamers, Marcelo L.; Engler Adam J. The dissertation author was the primary investigator and author of this material.

VITA

2018	Teaching Assistant, Cornell University
2018	Bachelor of Science (cum laude), Cornell University
2021	Teaching Assistant, University of California San Diego
2019-2024	Graduate Student Researcher, University of California San Diego
2024	Doctor of Philosophy, University of California San Diego

PUBLICATIONS

Suh, Y. J., Hall, M. S., Huang, Y. L., Moon, S. Y., Song, W., Ma, M., Bonassar, L. J., Segall, J. E., & Wu, M.. (2019). Glycation of collagen matrices promotes breast tumor cell invasion. Integrative Biology, 11(3), 109–117. https://doi.org/10.1093/intbio/zyz011

Moon, S. Y., De Campos, P. S., Matte, B. F., Placone, J. K., Zanella, V. G., Martins, M. D., Lamers, M. L., & Engler, A. J.. (2023). Cell contractility drives mechanical memory of oral squamous cell carcinoma. Molecular Biology of the Cell, 34(9). https://doi.org/10.1091/mbc.e22-07-0266

FIELDS OF STUDY

Major Field: Engineering

Studies in Bioengineering
Professor Adam J. Engler

ABSTRACT OF THE DISSERTATION

Oral Squamous Cell Carcinoma (OSCC) Learn from Tumor Micro-Environment to be Metastatic

by

So Youn Moon

Doctor of Philosophy in Bioengineering

University of California San Diego, 2024

Professor Adam J. Engler, Chair

As Oral Squamous Cell Carcinoma's (OSCC) patients' survival rate significantly decreases with metastasis, risk factors that can enhance OSCC metastasis should be identified and targeted. In this thesis, metastasis-inducing tumor-TME interaction is categorized into two – cell-extra-cellular matrices (ECM) and intra-tumor heterotypic cell-cell interactions – and studied

Tumor Matrix stiffening is ubiquitous in solid tumors and can direct epithelial-mesenchymal transition (EMT) and cancer cell migration. Stiffened niche can even cause poorly invasive OSCC cell lines to acquire a less adherent, more migratory phenotype, but mechanisms and durability of this acquired "mechanical memory" are unclear. Here, we observed that contractility and its downstream signals could underlie memory acquisition;

invasive SCC25 cells overexpress myosin II (vs. non-invasive Cal27 cells) consistent with OSCC. However, prolonged exposure of Cal27 cells to a stiff niche or contractile agonists upregulated myosin and EMT markers and enabled them to migrate as fast as SCC25 cells, which persisted even when the niche softened and indicated “memory” of their prior niche. Stiffness-mediated mesenchymal phenotype acquisition required AKT signaling and was also observed in patient samples, whereas phenotype recall on soft substrates required focal adhesion kinase (FAK) activity. Phenotype durability was further observed in transcriptomic differences between pre-conditioned Cal27 cells cultured without or with FAK or AKT antagonists, and such transcriptional differences corresponded to discrepant patient outcomes.

Tumor is made up of heterotypic cell populations and they can interact to affect each other’s behavior. OSCC showed response to cytokines from immune cells, but such cell-cell interaction within tumor has not been studied enough. Two heterotypic OSCC cell lines with different invasiveness – SCC25 and Cal27 – are indirectly co-cultured in this study to observe paracrine cell signaling between two cell lines. Cultured with SCC25-conditioned media (CM), Cal27 showed enhanced cell migration and transcriptomic changes related to cytokine response. SCC25-CM had higher expression of IL-1a, IL-6, IL-8, Angiogenin and PAI-1, and supplementing normal growth media with those cytokines comparatively increased Cal27’s motility. In response to the cytokines rich in SCC25-CM, Cal27 activate MAPK signaling pathways, and inhibition of the pathway disturbed cell migration enhancement by paracrine cell signaling.

Chapter 1 CELL CONTRACTILITY DRIVES MECHANICAL MEMORY OF ORAL SQUAMOUS CELL CARCINOMA (OSCC)

1.1 Introduction

There are more than 350,000 new oral and pharynx cancer cases and 177,000 deaths annually worldwide, and oral squamous cell carcinoma (OSCC) represents 80–90% of all malignant tumors of the oral cavity (Jensen et al., 2019; Johnson et al., 2011; Pires et al., 2013) with a 5-year survival rate that varies from 40 to 63% (Kamangar et al., 2006; Montero & Patel, 2015; Scully & Bagan, 2009; Warnakulasuriya, 2009). Oral lesions are clinically characterized by dysplastic regions with irregular rigid margins (Chi et al., 2015). Extracellular matrix (ECM) upregulation and crosslinking–relative to softer tumor adjacent epithelium (TAE)–creates the stiff tumor border, which has been observed in a variety of other tumors including OSCC (Bonnans et al., 2014; Boudreau et al., 2012; Frantz et al., 2010; Lu et al., 2012; Yu et al., 2019). ECM upregulation is correlated with poor patient outcomes (Burgstaller et al., 2017; Matte et al., 2019; Wei et al., 2015) and increased invasive potential (Chaudhuri et al., 2014; Ondeck et al., 2019; Paszek et al., 2005; Wei et al., 2015), but to date in the context of OSCC, this link and the mechanisms that regulate it has not been clearly articulated.

For cancer cells to sense and respond to ECM stiffness, communication between extracellular and intracellular compartments is necessary (Hanahan & Weinberg, 2011; Pickup et al., 2014). These compartments are mechanically linked by transmembrane integrins that connect the ECM with actin cytoskeleton and ultimately the nucleus via adhesion, contractile and signaling proteins (Parsons et al., 2010). While stiffness sensing mechanisms are well established in other cancers, e.g., kinases in breast (Calvo et al., 2013; Fattet et al., 2020; Levental et al., 2009), brain (Liu et al., 2018; Umesh et al., 2014; Wong et al., 2015), and ovarian (Wei et al., 2021) cancers among others, relatively little is known about OSCC.

Typically, these outside-in mechanisms establish a positive feedback loop whereby non-muscle myosin-II (NMM2) contractility modulates adhesions and integrin/ECM binding to further enhance signaling, contraction, and migration (Vicente-Manzanares et al., 2008; Wu et al., 2009). Stiffness-mediated signaling can result in cytoskeletal assembly changes and force transduction to the nucleus, which impacts gene transcription and epithelial-mesenchymal transition (EMT) (Chin et al., 2016; Stowers et al., 2019; Wang et al., 2009). For example, stiffer substrates can induce tumorigenesis in mammary epithelial cells via altered chromatin accessibility resulting from hypercontractile cells (Stowers et al., 2019). In lung tumors, stiffness enhances expression of EMT genes (Alonso-Nocelo et al., 2018; Tilghman et al., 2010). These dynamic interactions can even enhance tumor growth, survival and invasion (Butcher et al., 2009; Geiger et al., 2001; Paszek et al., 2005).

Once outside of their stiffened niche, however, cancer cells must also be able to maintain their stiffness induced EMT, i.e., invading mesenchymal-like cells retain marker expression and migratory potential. This ability to form “mechanical memories” has been shown in mammary epithelial cells, which after pre-conditioning on a stiff matrix, migrate faster, upregulate contractile proteins, and maintain EMT on a soft matrix (Nasrollahi et al., 2017). In dynamic contexts though, signaling becomes more complicated; in multi-cellular mammary spheroids or in matrix that stiffens with time, multiple redundant signaling pathways may collectively regulate EMT in mammary epithelial cells (Ondeck et al., 2019). We previously showed that poorly invasive OSCC cell lines can acquire a more migratory phenotype in a stiffer environment (Matte et al., 2019), i.e., 20 kiloPascal (kPa) which mirrors the stiffest regions of dysplastic oral tumors (Zhang et al., 2020). How such oral cells develop stiffness-mediated responses and whether they retain “memory” of their tumor-like niche when on softer matrix, i.e., 0.5 kPa, has not been thoroughly explored in OSCC. Herein, we demonstrate that a non-invasive oral epithelial cell line, i.e., Cal27, can undergo EMT and acquire “memory” from stiff matrix that

enables cells to maintain their new phenotype despite being on a softer niche. AKT and FAK play key roles in this process, which could be maintained for days in culture and are reflect in transcriptomic differences that corresponded to patient outcomes.

1.2 Results

1.2.1 Contractility regulates the acquisition of mechanical memory

Increased cell contractility typically occurs as a result of EMT (Aguilar-Cuenca et al., 2014; Friedl et al., 2012; Newell-Litwa et al., 2015; Parsons et al., 2010), but it is unclear in OSCC. To establish to what extent and where contractile machinery is present in OSCC and their derivative cell lines, we analyzed non-muscle myosin isoform expression in OSCC biopsies. NMM2B was detected at the basal cell layer and staining was strongest in cells at the invasive front of the tumor (**Figure 1.1A, S1**). Both patients–being of advanced stage IV– corroborate prior findings that tumors of more advanced TNM stages express higher NMM2B (Dias et al., 2019). In oral cell lines, NMM2A and B were expressed more in mesenchymal SCC25 vs. epithelial Cal27 cells (**Figure 1.1B**). To study how contractile machinery plays role in Cal27 acquiring mesenchymal-like phenotypes from stiff environment (Matte et al., 2019), lysophosphatidic acid (LPA), which stimulates contraction through its receptor's downstream signaling via Rho/RCK, and Blebbistatin, a non-muscle myosin inhibitor, were used along with exposure to substrates with varying stiffness. Culture of epithelial Cal27 cells on stiffer matrix or with LPA had similar effects on morphology and phenotype, leading to more compact cell colonies and higher EMT marker expression, versus culture on soft matrix or with Blebbistatin (**Figure 1.1C-D**). These results together suggest that the acquisition of more mesenchymal-like behavior, concurrent with our prior observations (Matte et al., 2019), may be the result of higher myosin and EMT marker expression.

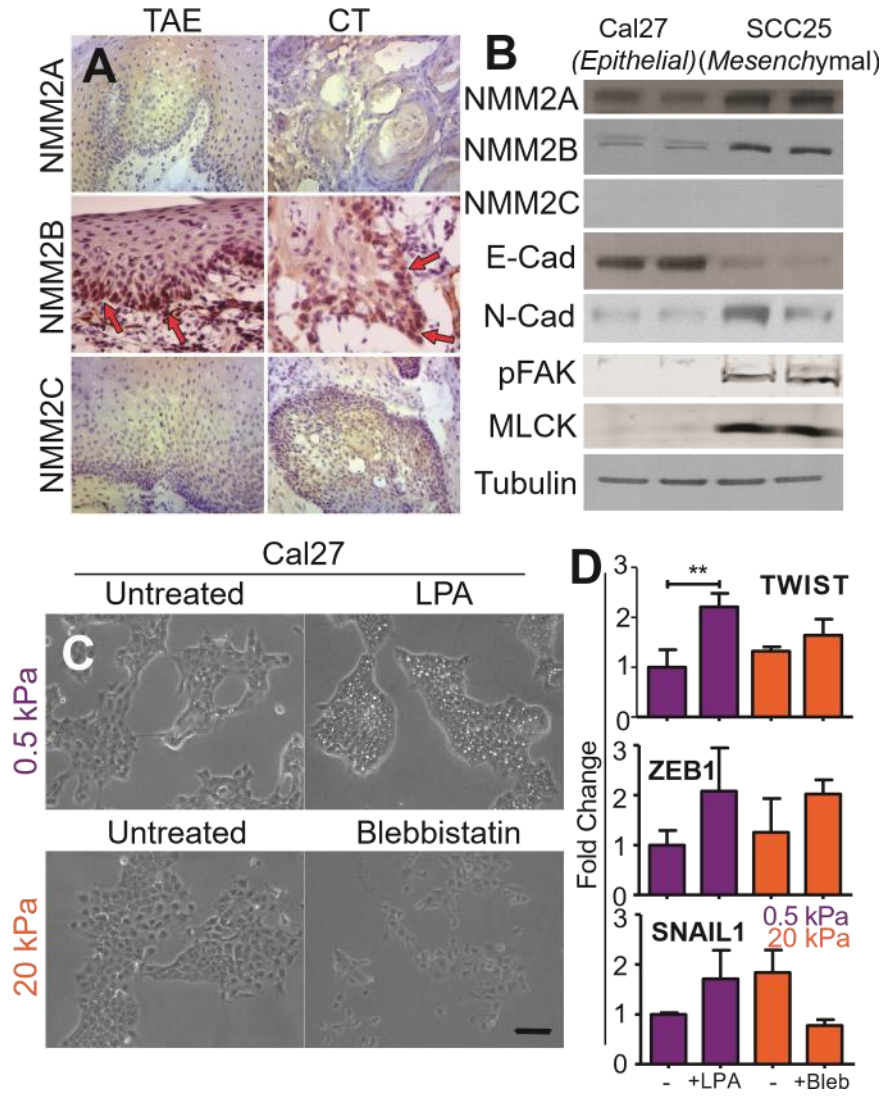


Figure 1.1: Contractility modifies cell behavior in oral squamous carcinoma in vivo and increases EMT marker expression in vitro
(A) Immunohistochemistry staining for non-muscle myosin (NMM) IIA, IIB and IIC in tumor adjacent epithelia (TAE) and center of the tumor (CT). Red arrows indicate positive staining (brown) (n=15). (B) Representative western blots for NMM 2A, 2B, and 2C as well as E-cadherin, N-cadherin and tubulin in low (Cal27; epithelial) or high (SCC25; mesenchymal) invasive OSCC cell lines. (C) Brightfield images of Cal27 cells after 5 days of culture on soft (0.5 kPa) or stiff substrates. Cells were selectively treated with Blebbistatin (10 μM) and LPA (10 μM) as indicated. Scale bar is 100 μm. (D) Fold change to mRNA expression is plotted for the indicated transcription factors, substrate stiffness (purple = 0.5 kPa; orange = 20 kPa), and drug treatment. All data is shown from triplicate biological replicates and was normalized to GAPDH and then to the soft control (0.5 kPa; far left). *p<0.01 via one-way ANOVA with Tukey's post-test.

Invasion requires that cells leave the tumor niche. Hence they must have durable expression of stiffness mediated EMT markers once in the tumor adjacent epithelium, i.e.,

“mechanical memory;” while present in other carcinomas (Nasrollahi et al., 2017), we sought to test this in OSCC cell lines and assess the impact contractility has on memory. Cal27 cells were conditioned on soft or stiff substrates for 5 days and replated onto soft substrate for an additional day (**Figure 1.2A**). Relative to mesenchymal SCC25 cells, we found E-cadherin peripheral localization was highest in Cal27 cells on soft matrix, which is an indicator of an epithelial phenotype, and was markedly reduced for cells pre-conditioned on stiff matrix. Conversely, those cells pre-conditioned on stiff substrates had statistically higher NMM2A expression than their soft substrate counterparts and were not different from mesenchymal SCC25 cells (**Figure 1.2B-D**). This reciprocal relationship suggests that stiff pre-conditioning could enable cells to acquire and maintain their prior mesenchymal phenotype despite tumor adjacent epithelium-like stiffness. This interpretation may also be consistent with cell migration after replating (**Figure 1.3A**); Cal27 cells pre-conditioned on a stiff niche or first treated with LPA retained higher migration velocity and explored a larger substrate area, whether migrating collectively or individually in 2D. Conversely when Cal27 cells were cultured with a contractile antagonist such as Blebbistatin after replating from a stiff to a soft hydrogel, cells typically responded by failing to maintain higher migration velocities (**Figure 1.3B-C**). These data, at least in 2D, suggest contractile regulation of mechanical sensing and maintenance of a stiffness-induced mesenchymal phenotype. Further consistent with this interpretation in 3D, pre-conditioned Cal27 cells were induced to form spheroids and then embedded into a collagen matrix. Those spheroids from cells plated originally on stiff hydrogels or that were treated with LPA were more invasive over 5 subsequent days of culture than their counterparts on soft matrix only or when cultured with Blebbistatin (**Figure 1.3D-E**). Taken together, 2D and 3D assays suggest that high cell contractility in soft environments may artificially induced mesenchymal-like responses that imply a sort of “mechanical memory” whereas contractile inhibition during pre-conditioning may block acquisition of such memory.

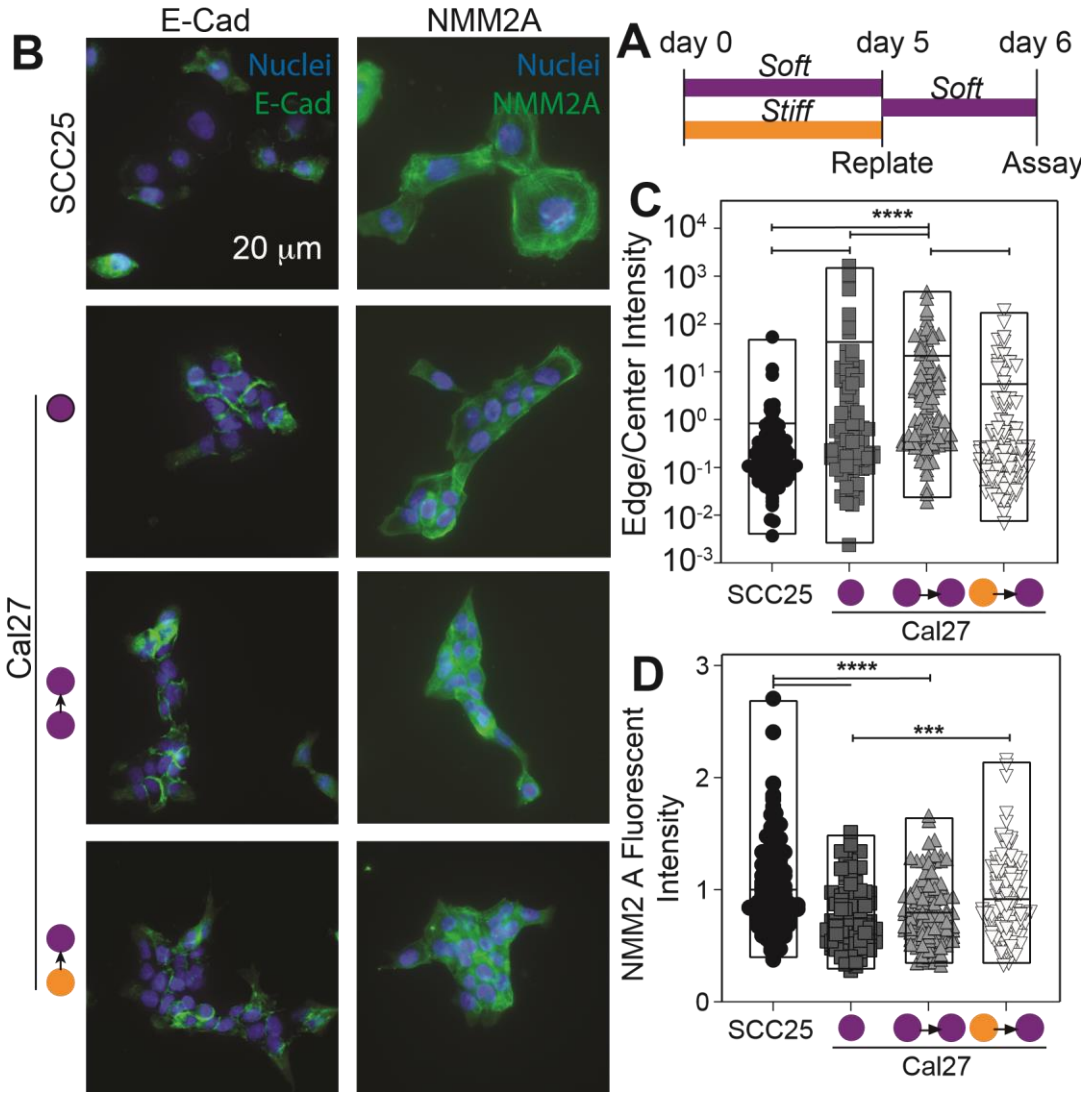


Figure 1.2: Stiffness-induced changes in E-Cadherin localization and NMM2 expression are durable in tissue adjacent epithelium-like stiffness.
(A) Experimental design of cell pre-conditioning and replating on stiff (orange) or soft (purple) substrates. (B) Immunofluorescence images are shown of SCC 25 cells (top) and Cal27 cells on soft substrate (top middle), without pre-conditioning (bottom middle), and with stiff pre-conditioning (bottom). Cells were stained in green for E-Cadherin (left column) and NMM2A (right column) and blue for nuclei (DAPI). Scale bar is 20 μm. Open arrowheads indicate cells with less peripheral E-cadherin or lower myosin expression whereas filled arrowheads indicate cells with more peripheral E-cadherin or higher myosin expression. (C) Plot of edge to center pixel intensity ratio for the conditions from panel B. Box plot shows mix, max, and mean values along with individual data points (n = 124, 112, 96, and 117, left to right, respectively). (D) Plot of NMM2A fluorescent intensity for the conditions from panel B. Data is normalized to average intensity of SCC25 for each biological replicate. Box plot shows mix, max, and mean values along with individual data points (n = 136, 126, 117, and 131, left to right, respectively). ***p<10-2, ****p<10-3 via one-way ANOVA with Tukey's post-test.

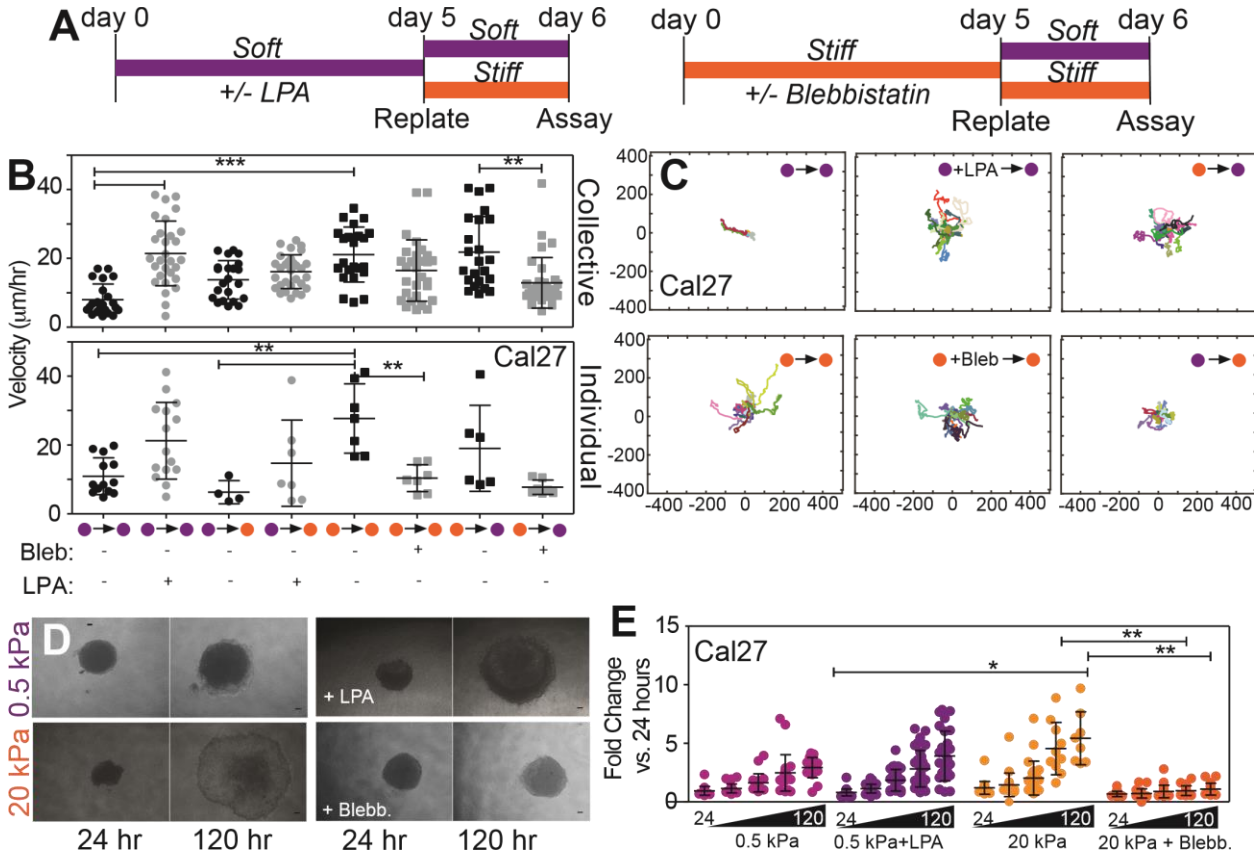


Figure 1.3: Acquisition of mechanical memory in 2D and 3D environment is affected by contractility.
(A) Experimental design of cell pre-conditioning and replating on stiff (orange) or soft (purple) substrates. (B) Collective (top) and individual (bottom) migration velocity was analyzed for Cal27 cells on stiffness combinations (soft=purple; stiff=orange) and/or treatment with LPA (10 μM) or Blebbistatin (10 μM) as indicated (n=22, 29, 22, 30, 23, 29, 23, and 32 cells for collective migration and n=13, 15, 4, 7, 7, 7, 6 and 7 cells for individual migration, left to right). (C) Rose plots of collective cell migration on stiffness combinations (soft=purple; stiff=orange) and/or treatment with LPA (10 μM) or Blebbistatin (10 μM) as indicated. Each line represents one cell trajectory. Axes indicate distance in μm. (C) Fold change to OSCC spheroids pre-conditioning in soft and stiff substrate (control and treated with LPA/Blebbistatin) normalized to 24h sphere. (D) Brightfield images at 24 and 120 hours of culture and (E) plots of OSCC-derived spheroid migration on soft (purple) or stiff (orange) substrates and treatment with LPA (10 μM) or Blebbistatin (10 μM) as indicated. Scale bar is 50 μm. *p<0.05, **p<0.01, ***p<0.001 for all data as analyzed by one-way ANOVA with Tukey's post-test.

1.2.2 Acquisition and recovery of mechanical memory, respectively, involves AKT and FAK signaling

To identify signaling pathway(s) involved in stiffness-mediated phenotype changes, we analyzed 43 phospho-proteins and found activity at 11 sites, i.e., signal >2-fold above

background, of which AKT (S308)–a pathway involved in OSCC migration (Fujii et al., 2020)–was the most phosphorylated when Cal27 cells that were maintained on soft matrix were replated onto stiff matrix for an hour. Conversely, Cal27 cells that were maintained on stiff matrix and then replated onto soft matrix for an hour had 23 sites above background; of those, FAK (Y397), which is required for OSCC stiffness-sensing (Zhang et al., 2021), was one of the most phosphorylated site when memories of the stiff substrate were "recalled" (**Figure 1.4A**). Contractility and signaling differences could cause larger transcriptomic differences between pre-conditioned Cal27 cells ("Learn") and those exposed to inhibitors ("Don't Learn/Forget"). RNA sequencing of these two groups revealed 822 differentially expressed genes (DEGs; $-0.1 > FC > 0.1$, $p\text{-val} < 0.1$) between "Learn" vs. "Don't Learn/Forget" groups (**Figure 1.4B; Table S1**). We mapped Gene Ontology (GO) terms onto these DEGs and found that the top 20 terms primarily associated with cellular components of the cytoskeleton and extracellular matrix and with biological processes associated with migration (**Figure 1.4C; Table S2**). 112 genes within the top GO terms were significantly and/or differentially expressed as highlighted by an MA plot (**Figure S2A, purple/green data; Table S3**). For 6 of the most significantly and/or differentially expressed genes (above/below or to the right of dashed lines in panel C; i.e., SDC4, ICAM1, FN1, and ITGAV for upregulated and RhoD and FSCN1 to be downregulated in "Learn" group), we further validated expression via qPCR, finding linear correlation between sequencing and qPCR (**Figure S2B**). Those significantly and/or differentially expressed genes (**Table S4**), which may form a minimal grouping of genes related to mechanical memory, were then used to stratify patients in The Cancer Genome Atlas (TCGA). To ensure a robust patient population, the expression profiles for all head-neck squamous carcinomas, including OSCC, were computed (n=155), and between the top and bottom expression quintiles, progression free interval (Figure 4D) and overall survival (**Figure 1.4E**) showed significant differences. These data suggest that there is perhaps a common transcriptomic signature that results from contractility-based pre-conditioning, which could be used to screen patient tumors for signs of "memory" in addition to

conventional histology.

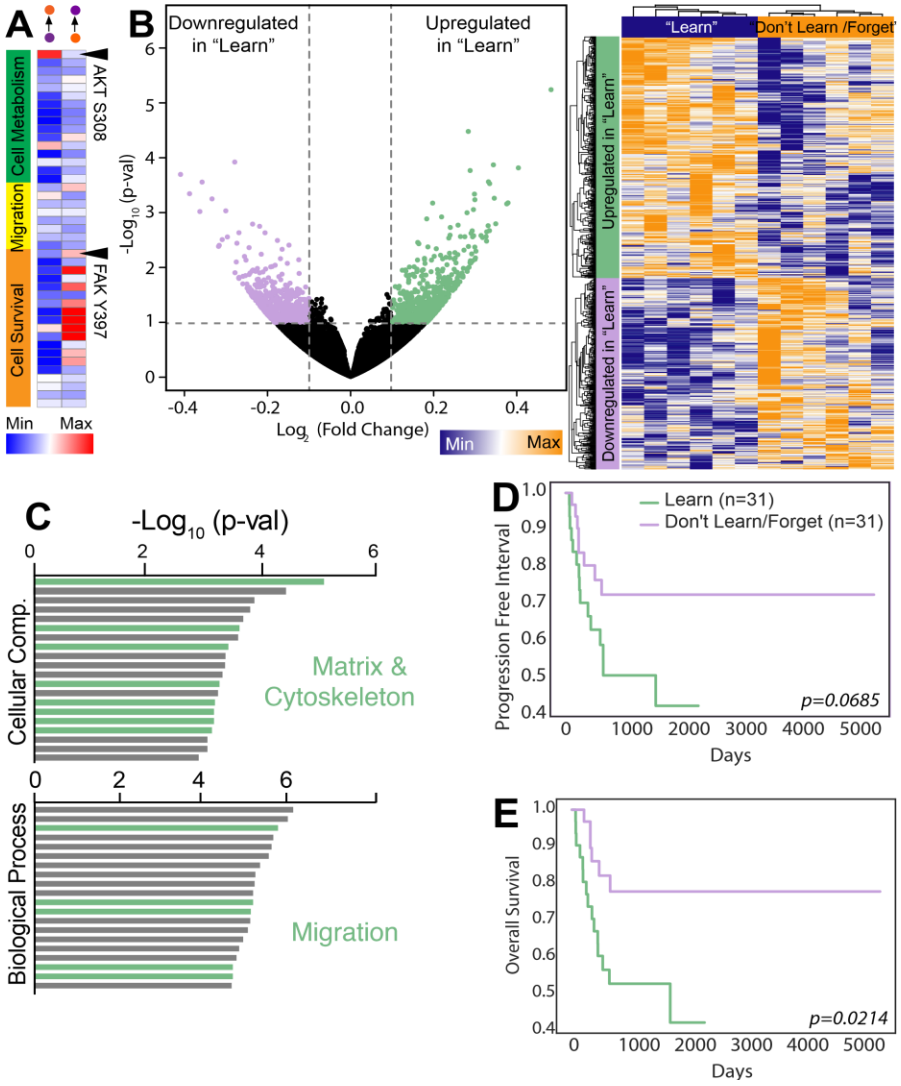


Figure 1.4: Mechanical memory involves AKT and FAK signaling
(A) Volcano plot (left) and heat map (right) of the genes from bulk RNA sequencing. In volcano plot, up(green)/down(purple)-regulated genes in "Learn" groups were identified and marked with log2 fold change of >0.1 and -log10 p-value > 1. Heatmap of shows the hierarchical clustering of differentially expressed genes identified from the volcano plot. (B) Gene ontological terms determined from DEGs in panel A. Terms shown in green indicate those associated with matrix & cytoskeleton (cellular component) and adhesion & migration (biological processes). (C) MA plot of expression versus fold change. Genes that were up or downregulated and that met the inclusion criteria from panel A are plotted as open data points. For the subset of genes that are also present in ontological terms in panel B, those up or downregulated genes are shown in green or purple, respectively. (D, E) Data above/below (i.e., (log2(fold change)>0.3) and/or to the right (i.e., log2(expression)>13) of dashed lines in panel C were identified as highly expressed or highly differentially expressed, were further validated in Figure S2, and used here to stratify patients in The Cancer Genome Atlas (TCGA). Plots show progression free interval and overall survival as indicated. Significance show in plots is based on a Log-Rank (Mantel-Cox) test.

Based on GO terms mapped on DEGs in which cell adherens junction and cell migration/motility are different between “Learn” vs. “Don’t Learn/Forget” (**Table S2**), cell adhesion and migration difference of Cal27 were assessed to study how AKT or FAK pathways are related to those cell functions and further affect mechanical memory acquisition processes. While adhesion strength was not significantly different (**Figure S3**), we found a titratable influence on migration; specifically, inhibition of AKT (5 μM AKT inhibitor) significantly reduced both collective and individual migration speed of cells conditioned on soft and then replated to stiff matrix (**Figure S4A**), and inhibition of FAK (10 μM FAK inhibitor) pathway discouraged cell migration after being replated from stiff to soft matrix (**Figure S4B**). When combined with stiff substrates or cultured with LPA, AKTi-treated Cal27 cells failed to “learn” or exhibit higher migration speed when replated (**Figure 1.5A**) similar to blocking contractility with Blebbistatin (**Figure 1.5B**). Conversely, replated Cal27 cells that were then treated with FAKi also failed to exhibit higher migration speed (**Figure 1.5A-B**) or could not recall the impact of prior mesenchymal transitions and “forgot.” Thus, both groups–one with impaired contractility and the other with an inhibited signaling pathway which upregulated during memory recovery–had significantly slower cell migration speed than the group conditioned on stiff substrates.

Validation of this mechanism in human tumors is critical to establishing its importance, hence 19 OSCC tumors were assessed in their core and invasive zones for AKT phosphorylation (**Figure 1.5C**) and collagen organization (as a surrogate for tumor rigidity (Wei et al., 2015)). Tumor cores were generally positive for AKT phosphorylation at S308, independent of TNM tumor stage. However, when stratifying by stage and collagen organization, only stage III/IV tumors had statistically higher percentages of cells phosphorylating S308 on AKT in the core versus adjacent invasive zone. For lower staged tumors or those with disorganized collagen, even cells in the adjacent invasive zone had phosphorylated AKT(S308) (**Figure 1.5D**). The lack of phosphorylation differences suggest that

tumors may be soft enough that cells do not develop sufficient “memory” in the core, which could corroborate the involvement of AKT pathway in the memory learning process for stiff, high-grade tumors.

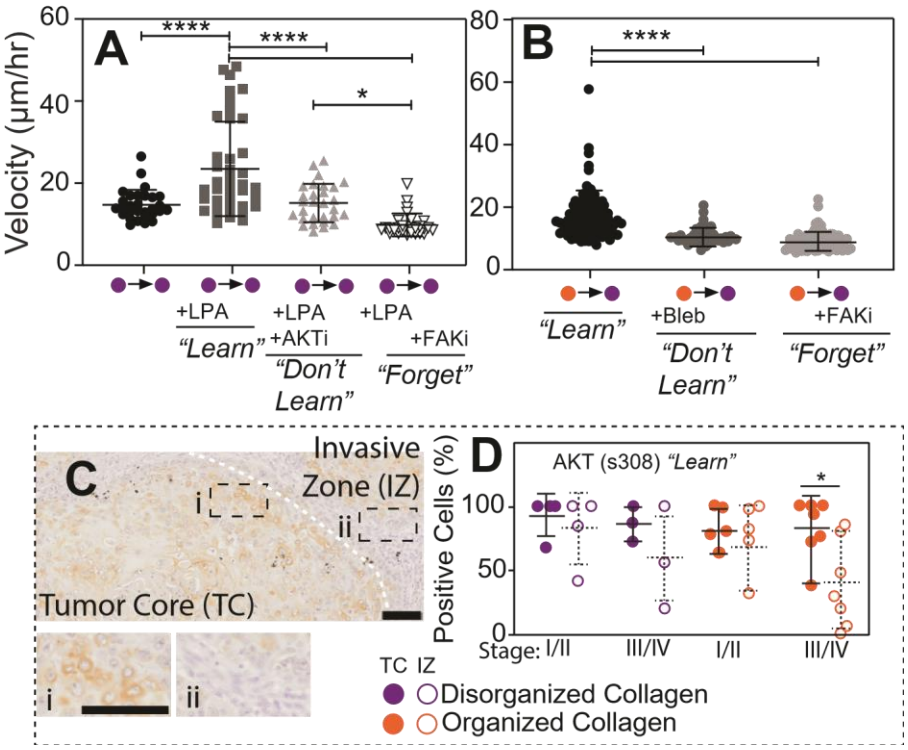


Figure 1.5: Transcriptomic differences between “Learn” vs. “Don’t Learn/Forget” groups. **(**A) Heat map of spot intensity from an array of 43 phosphorylation sites. Cal27 cell lysates were blotted, and cells had been switched from soft to stiff (“learn”; left) or stiff to soft substrate (“recall”; right) for 1 hour. Data is normalized to Cal27 cells cultured on their original substrate, i.e., soft and stiff, respectively. Red indicates up-regulation and blue indicates down-regulation relative to lysate from the original substrate. (B, C) Collective migration velocity was plotted for Cal27 cells on stiffness combinations as indicated (soft=purple; stiff=orange) plus selective treatment with AKT or FAK inhibitors, with contractile agonist LPA, or with contractile antagonist Blebbistatin as indicated. Below each condition is the term used for the memory state given the indicated treatment conditions. *p<0.05, ***p<0.0001 for all data as analyzed by one-way ANOVA with Tukey’s multiple comparisons test (n=29, 40, 29, and 28, left to right, respectively for panel B and n=59, 20, and 46¬¬¬, left to right, respectively for panel C). (D) Immunohistochemistry images of OSCC, noting tumor core (TC) and invasive boarder zone (IZ), which was stained for phosphorylated AKT(s308); white dashed line indicates the boarder. Inset images are shown and correspond to their regions i and ii in the TC and IZ, respectively. White arrowheads indicate positive staining in the inset image. Scale bar is 100 μm¬. (E) Plot indicating the percentage of positively staining cells per field for OSCC tumors based on their tumor grade. Data is sorted by the presence of organized collagen from SHG imaging, as a surrogate for stiff matrix (orange), or absence (purple) as well as location within the tumor, i.e., IZ (open data) and TC (filled data). Lines indicate average and standard deviation. *p<0.05 as analyzed by one-way ANOVA with Tukey’s multiple comparisons test.

1.3 Discussion

Bi-directional crosstalk between tumor cell and ECM can change cell behavior, thus ECM dynamics can modify cell phenotypes and promote malignancy (Van Helvert et al., 2018; Yamada & Sixt, 2019). Increased tissue stiffness is a well-known feature of tumors (Lu et al., 2012), and its potential to drive malignant transition in tumor cells has been studied in several tumor sites (Baker et al., 2013; Butcher et al., 2009; Chen et al., 2015). However, interaction between ECM stiffness and OSCC has not been deeply explored yet, so here we studied how OSCC cells are affected by matrix stiffness as its changes when transitioning from stiffer tumor to softer tumor adjacent epithelium (TAE). We had previously found that non-invasive Cal27 oral epithelial cells demonstrate increased cell migration velocity by being conditioned on stiff matrix (Matte et al., 2019), and here, we extended that work to observe that Cal27 cells pre-conditioned on stiff matrix not only adopt a more mesenchymal-like phenotype but also then maintain that expression for days more on softer substrates due to their prolonged ability to regulate contractility via AKT and FAK pathways. Not only did we then observe correlations with collagen organization differential AKT phosphorylation between tumor core and TAE, and tumor staging, but we also found that the stiff niche promoted a durable transcriptional change that correlated with patient outcomes.

While our data suggests that oral epithelial cell phenotype can be regulated by contractility, it is by no means a novel or exclusive mechanism. Contractile forces regulate a variety of processes ranging from embryogenesis to pathogenesis and are the result of cells modulating myosin activity (Butcher et al., 2009; Parsons et al., 2010; Wozniak & Chen, 2009). Within a cancer context, tumor progression has been shown to correlate with NMM2 expression, enabling cell migration and accelerating turnover of cell-cell adhesion (Peglion et al., 2014). We previously found a similar inverse relationship between adhesion and contraction when Cal27

cells were conditioned by stiffness for 5 days (Matte et al., 2019) as well as in breast cancer cells sorted by adhesion. There, less adhesive cells had more adhesion turnover and higher and more dynamic contractility, which make them more propulsive (Beri et al., 2020) and able to sense and migrated against mechanical gradients (Yeoman et al., 2021) relative to more strongly adherent cells. This process is also aided by supporting cells, e.g., cancer associated fibroblasts, which use traction forces generated by NMM2 to align and stiffen matrix to facilitate tumor invasion by the same mechanisms (Erdogan et al., 2017). While stiffness-based observations have occurred over the last decade, there is even more evidence from chemical modulation of contractility. LPA enhances ovarian (Sawada et al., 2002). and prostate (Wang et al., 2004) cell migration and invasion via Rho and ROCK in a manner that similarly regulates focal adhesion dynamics. We found that NMM2A expression increased after epithelial Cal27 cells were conditioned by LPA, which also made them more mesenchymal, migratory, and invasive, and conversely with Blebbistatin, blocking myosin activity prevented the mesenchymal phenotype. From these functional assays, we could conclude that cells can learn not only from the stiffness of matrix but also from contractility itself. More importantly for invasive, we further found that phenotype was maintained even in a new niche as “memory.” Matrix rigidity may also feedback on itself to enhance cell contractility (Huang & Ingber, 2005), so it is conceivable that Cal27 cells could continuously gain mechanical memory so long as they are in the stiff matrix of the tumor core, suggesting the cells that leave the tumor after increasing instruction could be even more virulent than their early disseminating counterparts. This concept, of course, would require significantly more complex in vivo labeling assays and tumor stiffness measurement to prove.

To understand how cells learn mechanical memory from the niche, we further examined which intracellular signaling pathways are involved. From the phospho-kinase array, we concluded that AKT and FAK signaling pathways are highly activated during memory learning

and recovery phase, respectively. AKT activation has been observed in OSCC cells where the TRPV4 (Ca2+-permeable nonselective cation channel) expression level was high (Fujii et al., 2020; Lee et al., 2017; Sharma et al., 2019). Since TRPV4 is mechano-sensitive, the activation cascade from TRPV4 to AKT signaling pathway could have been possible during 5 days of conditioning in stiff matrix. Here we found that AKT was necessary to acquire mechanical memory, since AKT inhibition decreased cell migration speed during pre-conditioning and in patients where phosphorylation was associated preferentially with tumor cores in the highest-grade tumors containing organized collagen. Conversely, we found that memory recovery in new niche depended on FAK phosphorylation. FAK has a critical function on adhesive complexes formation, cell shape, adhesion and motility (Lauffenburger & Horwitz, 1996; Mitra et al., 2005; Ridley et al., 2003). Highly activated FAK can also up-regulate Rho GTPases which enhances cytoskeleton organization (Mitra et al., 2005; Mitra & Schlaepfer, 2006; Seong et al., 2013). These features are all related to invasiveness of cells, and accordingly, mechanical memory remaining in the cell and recovered as a form of highly phosphorylated FAK allowed cells to keep invasive features.

Signals further downstream of kinases must ultimately result in transcriptional changes, which we found to correlate to patient outcomes, and are controlled by epigenetic marks in cells. As dysplastic regions evolve into invasive OSCC, cells acquire EMT markers, e.g., vimentin (Webber et al., 2017), concurrently with methylation at H3K4 (Rogenhofer et al., 2013) and H3K27 (Chen et al., 2013) but lose acetylation at H3K4 (Chen et al., 2013) and H3K9ac. OSCC tumors in the lowest and highest quartiles of percent H3K9ac+ cells showed markedly different disease outcomes (Webber et al., 2017). These data suggest that an acetylation-to-methylation switch accompanies disease progression, and it may be concurrent with the establishment of stiffness and memory. However further assessment beyond the work here is needed to determine if niche stiffness plays a role and which genes are affected. While these data suggest

that mechanical memory could involve histone modification, we believe that fundamentally our data here established a critical point; similar to other more well studied systems, e.g., breast (Nasrollahi et al., 2017), oral epithelial cells appear plastic, sensitive to stiffness, and after prolonged culture in stiffened niche, they retain a durable phenotype that is maintained in soft tumor adjacent epithelial, which could facilitate invasion.

1.4 Materials and Methods

Human Biopsies

The experimental design and the informed consent procedures were approved by the Ethical Committee of Federal University of Rio Grande do Sul - Brazil and of Hospital de Clínicas de Porto Alegre (HCPA) - Brazil (GPPG nº 11-0289; GPPG nº 14-0019) and all patients in this study provided written informed consent. Patients (n=19) with oral lesions were interviewed and submitted to surgery. OSCC diagnosis was confirmed histopathologically by a pathologist and fragments from regions corresponding to the center of the tumor, invasive zone, and the carcinoma edge tissue, i.e., tumor adjacent epithelia (TAE), were collected. Patient metadata are described in supplementary material (**Table S5**).

Cell Culture and Reagents

OSCC cell lines were a kind gift from Akihiro Sakai, University of California San Diego (UCSD). Cal27 cells were cultivated in DMEM high glucose (Gibco) supplemented with 10% fetal bovine serum (FBS) (Gemini Bio) and 1% penicillin/streptomycin (Gibco); SCC25 cells were maintained in DMEM/F12 with 15 mM HEPES (Teknova) supplemented with 10% FBS, 1% penicillin/streptomycin, and 400 ng/ml of hydrocortisone (Sigma). Cells were maintained in incubator at 37°C with 5% CO2. The cells were selectively treated with Blebbistatin (up to 10 μM, Cayman Chemical), Lysophosphatidic acid (LPA) (up to 10 μM, Enzo Life Sciences),

Perifosine, AKT inhibitor (0.5 and 5 μM, InvivoGen), and FAK inhibitor 14 (1 and 10 μM, Sigma-Aldrich).

Mechanical and Chemical Cell Conditioning on Polyacrylamide Hydrogels

Cal27 cells underwent 5 days of conditioning phase and a day of replating phase. After cells were seeded on collagen-coated polyacrylamide hydrogels (PA; 0.5 or 20 kPa), media was changed every day. PA hydrogels were fabricated and matrix proteins, e.g., collagen type I, were attached using well established protocols. Briefly, PA hydrogels were made on 12 mm or 25 mm glass coverslips that had been methacrylated by first oxidizing the surface through UV/ozone exposure (BioForce Nanosciences) followed by functionalization with 20 mM 3-(trimethoxysilyl)propyl methacrylate (Sigma-Aldrich, cat # 440159) in ethanol. A polymer solution containing either 3%/0.06% acrylamide/bis-acrylamide (Fisher) for 0.5 kPa hydrogels or 8%/0.264% for 20 kPa hydrogels, 1% v/v of 10% ammonium persulfate (Fisher), and 0.1% v/v of N,N,N′,N′-tetramethylethylenediamine (VWR) was prepared. 15 μl for 12 mm coverslips and 30 μl for 25 mm coverslips of hydrogel solution was sandwiched between a functionalized coverslip and a dichlorodimethylsilane-treated glass slide and polymerized for 10 and 30 minutes respectively for 20 kPa and 0.5 kPa gels. Hydrogels were incubated in 0.2 mg/ml sulfo-SANPAH (Fisher, cat #22589) in sterile 50 mM HEPES pH 8.5, activated with UV light (wavelength 350 nm, intensity 4 mW/cm2) for 10 min, washed three times in PBS, and then incubated in 150 μg/ml collagen solution (Corning) overnight at 37°C.

LPA, Blebbistatin, or Perifosin were also selectively applied during the conditioning phase. After 5 days of conditioning, cells were trypsinized with 0.25% trypsin-EDTA for 20 min at 37oC, 5% CO2 and replated on soft (0.5 kPa) gels to be incubated one more day at 37oC, 5% CO2. FAK inhibitor 14 was applied during replating phase.

Real-Time PCR

RNA was extracted from cells using using RNeasy Mini Kit (Qiagen) and total RNA quantity and quality was checked via A280/A260 ratio. Reverse transcription was performed with SuperScript IV Reverse Transcriptase (Thermo Fisher Scientific, #180090010) on 2 µg of RNA template. Quantitative PCR was performed (45 cycles, 95°C for 15 s followed by 60°C for 1 min) using a 7900HT Fast Real-Time PCR System (Thermo) with the primer sets described in Table S6 and PowerSYBR Green Supermix (Applied Biosystems, #436759). Target genes expressed in experimental groups were normalized with genes (including GAPDH as housekeeping gene) expressed in native Cal27 as control using delta-delta-Ct method.

Migration Assay

OSCC cells were plated on either 0.5 or 20 kPa PA hydrogels for 12h and were then imaged with a Nikon Eclipse Ti-S microscope equipped with a motorized temperature- and CO2-controlled stage. Cells were imaged at 10x in brightfield at multiple positions every 15 min for 24 h. For analysis of migration parameters, the nucleus of each migratory cell was used as a reference point to track each cell with the ‘Manual Tracking’ plugin on ImageJ. Migration was considered to be in single-cell mode when a cell did not touch any other cell during its migration movement. Migration was considered to be in collective-cell mode when cells migrated in a group of two or more cells.

Phospho-Kinase Array

Protein phosphorylation was examined using a membrane-based sandwich immunoassay (Proteome Profiler Array, R&D Systems, #ARY003C) according to the manufacturers' instructions. Briefly, total Cal27 cells were trypsinized after 5 days in soft (0.5 kPa) or stiff (20 kPa) substrate and re-plated in another stiffness for 1 h in 6-well plates. Cells plated in the same substrate after 5 days were used as a control. Lysates were made from

cultures and a total of 300 ug protein was then incubated with the Human Phospho-Kinase Array. The proteins present in a lysate sample were captured by discrete antibodies printed in duplicate across the nitrocellulose membranes. The array was washed 3X with buffer for 10 minutes on a rocking platform shaker and then incubated with a cocktail of biotinylated detection antibodies and subsequent application of streptavidin-HRP conjugate. The signals were detected with Chemi Reagent Mix (R&D Systems, Abingdon, Oxford, UK). Developed signals were analyzed using ImageJ analysis software.

Western Blotting

Cells were lysed with mRIPA buffer and total amount of protein was measured by BCA assay kit (Pierce; #23225). 10-15 µg of protein per sample was denatured by 4x Laemlli sample buffer and heated at 95℃ for 5 minutes. Samples were loaded to only 5% Bis-Tris gels and underwent electrophoresis under 140 V for 1.5 hour. Proteins on gel were blotted to nitrocellulose membrane using iBlot semi-dry transfer system (Invitrogen, #IB21000). The membrane was blocked for an hour at room temperature. The membrane were first immunoassayed with primary antibody at 4℃ for 24 hours to detect NMM2A (1:500, Cell Signaling, #3403), NMM2B (1:500, Cell Signaling, #8824), NMM2C (1:500, Cell Signaling, #8189), E-cadherin (1:1000, Cell Signaling, #3915), N-cadherin (1:1000, Cell Signaling, #13116), pFAK (1:1000, Cell Signaling, #3283), MLCK (1:1000, Sigma-Aldrich, #SAB4200808), and Tubulin (Sigma-Aldrich, #SAB4500088). After overnight incubation, the membrane was rinsed with buffer three times, 5 minutes per rinse. The membrane was incubated with Alexa Fluor 680 donkey anti-mouse (1:5000, Invitrogen, A10038) and Alexa Fluor 790 donkey anti-rabbit (1:5000, Invitrogen, A11374) diluted by blocking buffer for an hour at room temperature. Image was acquired by LI-COR Odyssey CLx imaging software and analyzed by Image Studio Lite.

Immunofluorescence

After conditioning and replating phase, Cal27 were fixed on the PAAGS (3.7% paraformaldehyde, 15 min, RT). In addition to conditioned cells, Cal27 and SCC25 were fixed after overnight incubation on gel to be used as control. Cells were washed with PBS (3x, 10 min each), permeabilized (30 min) with 0.5% Triton X in Solution A and blocked (30 min) with 0.1% Triton-X in buffer (0.3M Glycine, 10% FBS, and 1% Bovine Serum Albumin in Solution A). After rinsing (3x, 10 min each) with Solution A, anti-E-Cadherin (1:200, Cell Signaling, #3915) and anti-NMM2A (1:50, Cell Signaling, #3403) antibodies in IF buffer was applied to fixed samples and incubated overnight at 4oC. After rinsing with Solution A (3X, 10 min each), samples were selectively stained with anti-rabbit (1:500, 1:500, ThermoFisher, #A-11008) or anti-mouse (1:500, ThermoFisher, #A28175) secondary antibodies for 2 h at room temperature. Nuclei and actin staining was done with DAPI (1:1000, Tocris, #5748) and rhodamine-phalloidin (1:250, Cytoskeleton, Inc., #PHDR1) for 20min at room temperature on shaker. After staining, samples were rinsed once with 0.5% Triton X in solution A (5min), twice with solution A (10 min each), and once with DI water. Samples prepared on coverslip were mounted on microscope slide with fluoromount, and images were acquired by Keyence BZ-X800 microscope.

ImageJ was used to analyze immunofluorescent images. For E-cadherin-stained samples, images had their background subtracted. Then, the edge of each cell was traced in the actin channel and pixel intensity with respect to the radial distance from the center of the cell was measured in E-cadherin channel with “Radial Profile” plugin in ImageJ. Cells whose aspect ratio below 2 were used for analysis to remove the measurement error due to cell morphology. For each cell, pixel intensity for pixels within the first and last 5% of the cell radius were averaged and plotted as a ratio of edge/center. For NMM2-stained samples, average intensity per cell was plotted and normalized to the batch average for control SCC25 cells.

RNA Sequencing

RNA from Cal27 cells cultured in “learn” versus “don’t learn” or “forget” conditions was collected by RNeasy Minit Kit (QIAGEN, 74104). The purified RNA was then processed by the Institute for Genomic Medicine at University California San Diego. RNA integrity was analyzed using an Agilent Tape station system and precise RNA concentration determined using a Qubit 2.0 Fluorometer. Libraries were built using the Illumina TruSeq Stranded RNA, High Throughput Library Prep Kit and sequenced on a NovaSeq 6000 for samples with RIN numbers at 9.0 and above. RNA-Sequencing data was analyzed by ROSALIND® (https://rosalind.onramp.bio/), with a HyperScale architecture (ROSALIND, San Diego, CA). Reads were trimmed using cutadapt. Quality scores were assessed using FastQC. Reads were aligned to the human genome build dm6 using STAR. Individual sample reads were quantified using HTseq and normalized via Relative Log Expression (RLE) using DESeq2 R library. Enrichment was calculated relative to a set of background genes relevant for the experiment. Panther was used to assess GO terms for gene lists generated in Rosalind. DEseq2 was also used to calculate fold changes and p-values and perform optional covariate correction. Clustering of genes for the final heatmap of DEGs was done using the Partitioning Around Medoids method using the fpc R library. Functional enrichment analysis of pathways, gene ontology, domain structure and other ontologies was performed using HOMER.

The Cancer Genome Atlas Dataset Analysis

The Cancer Genome Atlas (TCGA) raw data were directly downloaded from NIH NCI GDC Data portal. Corresponding clinical metadata were obtained from a previous publication. Among the patient data with head-neck squamous carcinoma (HNSC), those whose primary site is either base of tongue or other and unspecified parts of tongue were used for analysis. The 5-year survival rate of patients were correlated with gene expression corresponding to “Learn” or “Don’t Learn/Forget”. Expression of the differentially expressed gene between “Learn” and

“Don’t Learn/Forget” subgroups were normalized by z-score based on the mean of each gene expression across the whole patient data. For every patient, z-score of all DEG were summed, and z-score based quintiles were mapped to “Learn” and “Don’t Learn/Forget” categories. The Kaplan-Meier method was used to create overall survival (OS) and progression free interval (PFI) comparing the top and bottom quantile of patient data. To determine the significance of survival rate difference between two groups, log-rank test was used. Survival analysis includes the Lifelines python library (https://lifelines.readthedocs.io/en/latest/).

Data Availability

Data generated in this study was deposited to NCBI under GEO207685. We do not impose any restrictions on data availability. Relevant scripts for the analysis of TCGA data are available at: https://github.com/englea52/OSCC_Memory.git

Statistics

All data is shown from triplicate biological replicates with the total number of measurements made indicated in figure legends. For qPCR gene expression, 2D migration assays, 3D spheroid invasion, and immunofluorescence and immunohistological quantification, data was analyzed by one-way ANOVA with Tukey’s post-test or multiple comparisons test as indicated. For all analyses, *$p<0.05$, **$p<0.01$, ***$p<0.001$, ****$p<0.0001$. Significance for TCGA analyses were performed with a Log-Rank (Mantel-Cox) test. Data expressed as box-and-whisker plots show all points with the mean and whisker ends corresponding to minimum and maximum values. All other values are expressed as mean +/- standard deviation. Statistical analyses were performed using Prism software.

Acknowledgements

Chapter 1, in full, is a reprint of the material as it appears in Cell Contractility Drives Mechanical Memory of Oral Squamous Cell Carcinoma. Moon, So Youn; Campos, Paloma S.; Matte, Bibiana F.; Placone, Jesse K.; Zanella, Virgi L. G.; Martins, Manoela D.; Lamers, Marcelo L.; Engler, Adam J., Molecular Biology of the Cell, 2023. The dissertation author was the primary investigator and author of this paper.

Chapter 2 PARACRINE INTRA-TUMOR CELL SIGNALING ENHANCES TUMOR METASTASIS IN ORAL SQUAMOUS CELL CARCINOMA (OSCC)

2.1 Introduction

Tumor interacts with tumor microenvironment (TME) which is spatially and temporally dynamic (Alamoud et al., 2018-05-17). Such interaction can lead to tumor cells behavioral change (Koontongkaew, 2013). Specifically, epithelial-to-mesenchymal transition (EMT)-driving tumor-TME interaction has been studied in various tumor sites as metastasis has negative impacts on prognostic outcome (Jing et al., 2011). Stiffened extra-cellular matrices (ECM) is one of the ubiquitous non-cellular characteristics in TME (Paszek et al., 2005) and is known to enhance cell migration (Kraning-Rush & Reinhart-King, 2012-5-1; Matte et al., 2019; Vasudevan et al., 2020/12/01). We previously studied that Oral Squamous Cell Carcinoma (OSCC) also reacts to stiff tumor matrix, and even non-invasive cell line (Cal27) demonstrates EMT like responses with increased contractility and motility (Matte et al., 2019). We further supported that invasiveness change in Cal27 can be maintained as mechanical memory within cells to demonstrate enhanced cell motility even when they are moved to soft substrate which mimics normal stromal tissue they are facing in the process of metastasis (Moon et al., 2023).

If metastatic property can be persisted as memory within cells, we wondered if that memory can be conveyed to other less invasive cells within tumor to induce EMT and migration. To study the possibility of memory transfer between cells, we should first understand how cell populations with different phenotypes communicate with each other in OSCC. Interaction among intra-tumor heterotypic cell populations has been studied in various tumor sites. Carey et al. (Carey et al., 2013) demonstrated with breast tumor and prostate adenocarcinoma multi-cellular spheroids that malignant cells readily invade through ECM and epithelial cells follow them. Direct co-culturing can change the invasiveness of epithelial cells as malignant cell lines

that lead invasive strands allow epithelial cells to trail behind.

Though the cells are not physically adjacent to each other, they can still interact in paracrine ways (Hoelzinger et al., 2007/11/07; Melzer et al., 2016-09-08; Sunami et al., 2022-01-31). Such interaction is exemplified in Glioblastoma multiforme (GBM) which is known to express truncated version of EGFR (EGFR vIII). When astrocytes expressing normal EGFR (wtEGFR) were cultured with media conditioned by EGFR vIII-expressing astrocytes, their adhesion strength decreased (Banisadr et al., 2020). Banisadr et al. argues that cytokine TNF-alpha, which demonstrated greater than 2-fold change in conditioned media, affected adhesive strength change in wild type cells. Paracrine cell signaling affecting cell behavior is also studied between OSCC and macrophages (Alves et al., 2021). However, such interaction within OSCC between heterotypic tumor cell populations has not been studied enough. By studying paracrine signaling between two heterotypic OSCC cell lines, we would like to highlight a chance of which invasiveness that tumor cells learned from ECM can be transmitted from cells to cells to effectively increase the whole tumor's malignancy.

In this paper, we demonstrate that non-invasive OSCC cell line (Cal27) can undergo EMT as they are indirectly co-cultured with invasive cell line (SCC25) via conditioned media (CM). In this metastasis-inducing paracrine cell-cell interaction, cytokines – Interleukin (IL)-1a, IL6, IL-8, Angiogenin, and Plasminogen activator inhibitor-1 (PAI-1) – secreted by invasive cell line play role. The involvement of 5 cytokines is supported by proteomic analysis of the SCC25-CM and functional/transcriptomic analysis of Cal27 cultured with that media. Our hypothesis is also reflected on patient outcomes in which the group with up-regulation of given cytokines has lower 5-year survival rate. MAPK and AKT are studied to be upregulated in response to the cytokines, so each pathway was inhibited during indirect co-culturing for further study of downstream pathways.

2.2 Results and Discussion

2.2.1 Paracrine Cell Signaling between Invasive and Non-Invasive Cell Populations in OSCC can Make Non-Invasive Cells be Invasive

To study paracrine cell signaling between invasive and non-invasive cell populations in OSCC, an indirect co-culturing assay using conditioned media (CM) was designed (**Figure 2.1A**). Non-invasive cell line of OSCC (Cal27) was incubated with SCC25 growth media (GM) (DMEM/F12 1:1 with 10% FBS, 1% penicillin/streptomycin, and 400 ng/ml hydrocortisone) conditioned with SCC25 on plastic tissue culture plate (SCC25-CM) or SCC25 on soft (0.48 kPa PA gel) substrate (SCC25 gel-CM). Cal27 incubated with Cal27 growth media (Cal27-GM) on either soft or stiff (20 kPa PA gel) served as a negative and positive controls to compare the effect of SCC25-CM on Cal27 motility. Besides Cal27-GM, Cal27 on soft substrate was also incubated with fresh SCC25 growth media (SCC25-GM), since two cell lines use different types of growth media.

Both media type and the incubation time affected Cal27's cell migration speed (**Figure S6**). Regardless of the substrate on which SCC25 was seeded during conditioned media preparation, Cal27 cultured with either SCC25-CM or SCC25 gel-CM showed enhanced cell migration speed from the third day of incubation (**Figure 2.1D-E**). Matte et al.'s study (2019) has shown that EMT transcription factors or cadherins expression in SCC25 did not change with respect to the stiffness of the substrate. Accordingly, SCC25 on different substrates could have made conditioned media with similar profile – at least, motility-wise – which explains the comparable result of cell migration speed enhancement between SCC25-CM and SCC25 gel-CM cultured Cal27. Such trend and extent of migration speed increase was similar to Cal27 seeded on stiff substrate (**Figure 2.1F**), whose response to stiffened extracellular matrices has previously been studied (Matte et al., 2019; Moon et al., 2023). On the other hand, Cal27

cultured with fresh GM (either Cal27-GM or SCC25-GM) showed no or slight change in cell migration speed (**Figure 2.1B-C**). Since comparison between two different media types caused slight difference in Cal27 cell behavior, we decided to use Cal27 in SCC25-GM as a base control through the study.

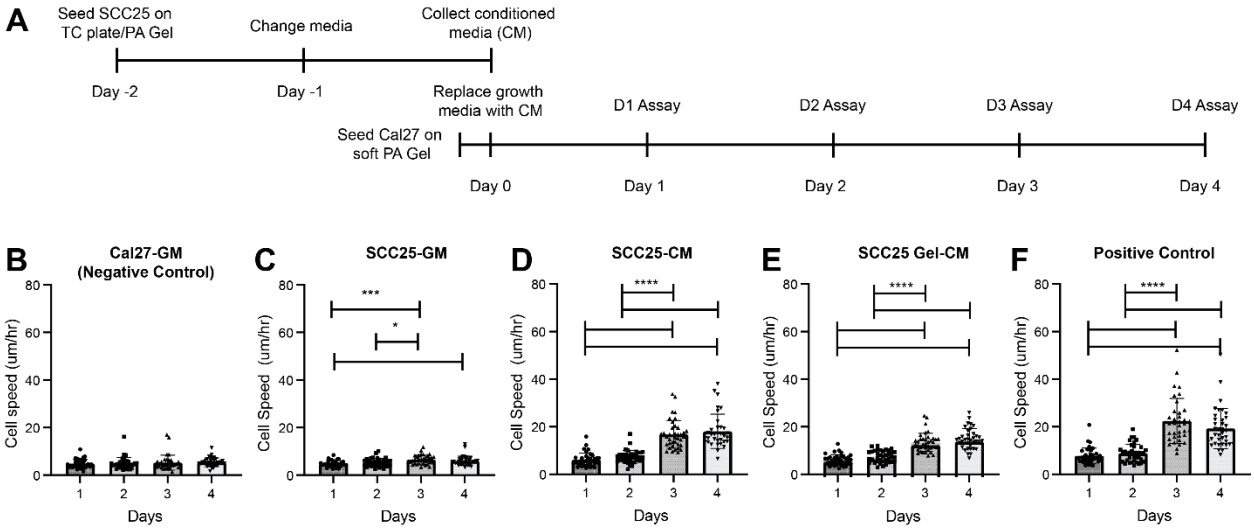


Figure 2.1: Motility change in Cal27 after indirect co-culturing with SCC25 using conditioned media (CM).
(A) Experimental design of SCC25-CM preparation and indirect co-culturing of Cal27 with SCC25 using the conditioned media. Cal27's motility measurement for 4 days of culturing on soft PA gel with (B) Cal27-GM, (C) SCC25-GM, (D) SCC25-CM, and (E) SCC25 Gel-CM. (F) Motility measurement of Cal27 on stiff PA gel with Cal27-GM as a positive control. *p<0.05, **p<0.01, ***p<0.001, ****p<0.0001 for all data as analyzed by one-way ANOVA with Tukey's multiple comparison test.

To study transcriptomic change as Cal27 is exposed to SCC25-CM, RNA sequencing data of Cal27 incubated with SCC25-CM for 3 days were analyzed with respect to Cal27 with SCC25-GM for a day. With -1.5 and 1.5 of log fold change (lfc) threshold, and 0.05 of p-adj threshold, Cal27 indirectly co-cultured with SCC25 revealed 134 differentially expressed genes (DEGs) (**Figure 2.2A-B**). We mapped top 98 Gene Ontology (GO) terms onto these DEGs (**Figure 2.2C**) and 12 of biological processes terms were associated with cell response to cytokine and intra-cellular signaling pathways. With RNA-sequencing and related GO term analysis, we hypothesized that cytokines are involved in metastasis-inducing paracrine cell-cell

interaction. This is in line with the study about GBM (Banisadr et al., 2020) in which wild type astrocytes respond to TNF-alpha highly expressed in EGFRvIII-expressing astrocytes-conditioned media and the study of OSCC and macrophages crosstalk via cytokines.

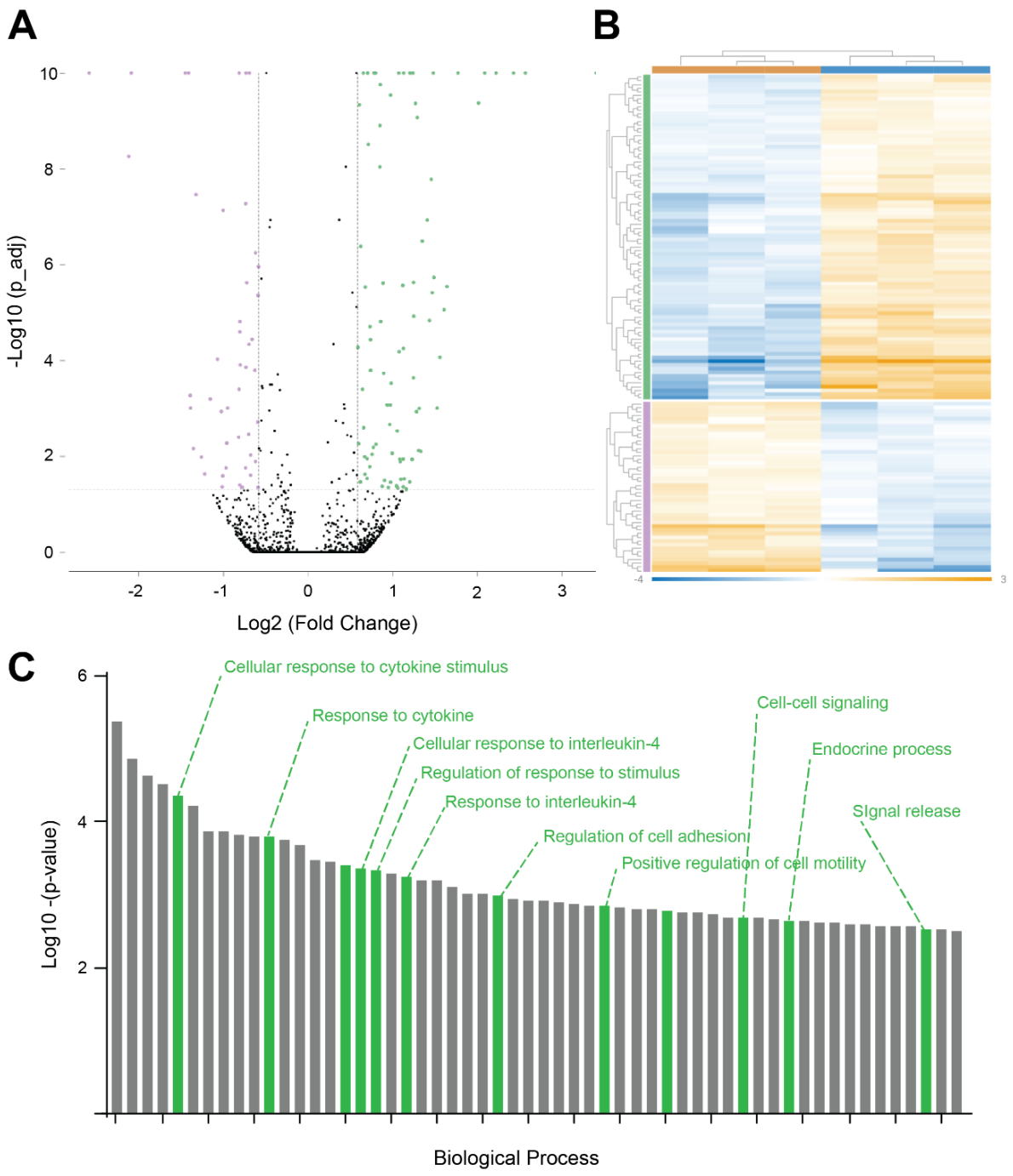


Figure 2.2: Transcriptomic change in Cal27 after being cultured with SCC25-CM for 3 days
Volcano plot (A) and heat map (B) of the genes from bulk RNA sequencing comparing Cal27 cultured with SCC25-CM for 3 days vs. with SCC25-GM for a day. DEGs in volcano plot were filtered with log2 fold change of >0.15 (up-regulated) or <-0.15 (down-regulated) and -log10(p-value) > 1. Hierarchical clustering of DEGs are shown in the heat map. (C) Biological process Gene Ontology (GO) terms based on DEGs. The terms related to cytokine response or cell motility change are marked green.

2.2.2 Cytokines – IL-1a, IL-6, IL-8, Angiogenin, and PAI-1 – are involved in Metastasis-Inducing Paracrine Cell Signaling

To reveal cytokines responsible for the enhancement of Cal27 motility, we studied cytokine profile of conditioned media: SCC25-CM, Cal27 soft-CM, and Cal27 on stiff-CM. Cal27 soft-CM is used as a control here to reflect autocrine signaling as Cal27 is cultured with fresh media. Cal27 on stiff substrate is included in this cytokine profiling, as the cell line's epithelial to mesenchymal transition (EMT)-like response to stiff substrate is shown in previous study (Matte et al., 2019), and moreover, Cal27's motility enhancement by SCC25-CM and stiff substrate had similar trend. Base media for all three conditioned media was SCC25-GM, so cytokine expression was normalized by fresh SCC25-GM's cytokine array result. Log fold change of cytokine expression in conditioned media was plotted as a heat map (**Figure 2.3A**). For cytokines with opposite expression profile between SCC25-CM and Cal27 soft-CM, all of them but one – GDF-15 – were up-regulated in SCC25-CM while down-regulated in Cal27 soft-CM. We focused on the cytokines which are up-regulated in both SCC25-CM and Cal27 stiff-CM : GM-CSF, IGFBP-3, IL-8, Thrombospondin-1, Angiogenin, Lipocalin-2, and PAI-1. We also took DEGs from RNA sequencing into consideration to identify the cytokines of interest. Ingenuity Pathway Analysis (IPA) from QIAGEN figured out upstream regulators that are likely to be activated or inhibited (**Figure 2.3B**) based on DEGs (**Figure 2.2A**). Among 12 upstream regulators identified by IPA, 3 cytokines – IL-1a, IL-17A, and IL-6 – showed up-regulation in SCC25-CM cytokine array.

10 cytokines were further validated with enzyme-linked immunosorbent assay (ELISA) (**Figure S7**). The concentration of GM-CSF (**Figure S7A**), Thrombospondin-1 (**Figure S7D**), and IL-17A (**Figure S7I**) were similar between SCC25-CM and Cal27 soft-CM. The expression of IGFBP-3 (**Figure S7B**) and Lipocalin-2 (**Figure S7F**) was rather higher in Cal27 soft-CM than in SCC25-CM. The expression of 5 cytokines – IL-1a (**Figure S7H**), IL-6 (**Figure S7J**), IL-8

(**Figure S7C**), Angiogenin (**Figure S7E**), and PAI-1 (**Figure S7G**) – quantified by ELISA agreed with the trend shown in cytokine array.

To functionally study the involvement of cytokines in metastasis-inducing paracrine cell-cell interaction, depletion of cytokines from conditioned media with immunoprecipitation was attempted. To deplete IL-8, SCC25-CM was incubated with IL-8 antibodies overnight, and the antibodies were pulled down with magnetic beads. After immunoprecipitation, the concentration of IL-8 in SCC25-CM decreased significantly to near complete depletion (**Figure S7C**). Though Cal27cultured with IL-8-depleted SCC25-CM showed enhanced cell migration speed after 3 days, the enhancement was not as large as that of Cal27 cultured with SCC25-CM with IL-8 (**Figure 2.3C-D**). This depletion assay suggests that IL-8 is a necessary condition for cell-cell interaction in terms of cell migration propensity but not sufficient. Depletion of conditioned media was also attempted for other cytokines – Angiogenin and PAI-1. Though we diluted the conditioned media and maxed out the amount of antibodies that can be conjugated to magnetic beads, PAI-1 could not be depleted from the conditioned media at all (**Figure S7G**). Angiogenin could be partially depleted, but the remaining amount of the cytokine was still 60% of the one before depletion (**Figure S7E**). Since more than half amount is remaining in the media, the depletion method cannot completely clear the effect of cytokines on cell behavior.

Instead of depletion, we decided to supplement SCC25-GM with cytokines to make it like SCC25-CM. Titration of cytokines from 1 to 100 ng/ml demonstrated that 1ng/ml of each cytokine in growth media altogether is enough to enhance cell motility to the level of those cultured with SCC25-CM (**Figure S8**). SCC25-GM was supplemented with each cytokine individually to understand the role of each in paracrine interaction. Once growth media is supplemented by either of 5 cytokines, Cal27 cultured with the media demonstrated increased cell migration speed than those cultured with fresh SCC25-GM. However, the amount of

enhancement was not as high as those cultured with growth media supplemented by all 5 cytokines, SCC25-CM, or Cal27 cultured on stiff substrate (**Figure 2.3E**). We concluded that 5 cytokines we listed are all necessary condition for metastasis-inducing paracrine cell signaling, but each one of them cannot be sufficient.

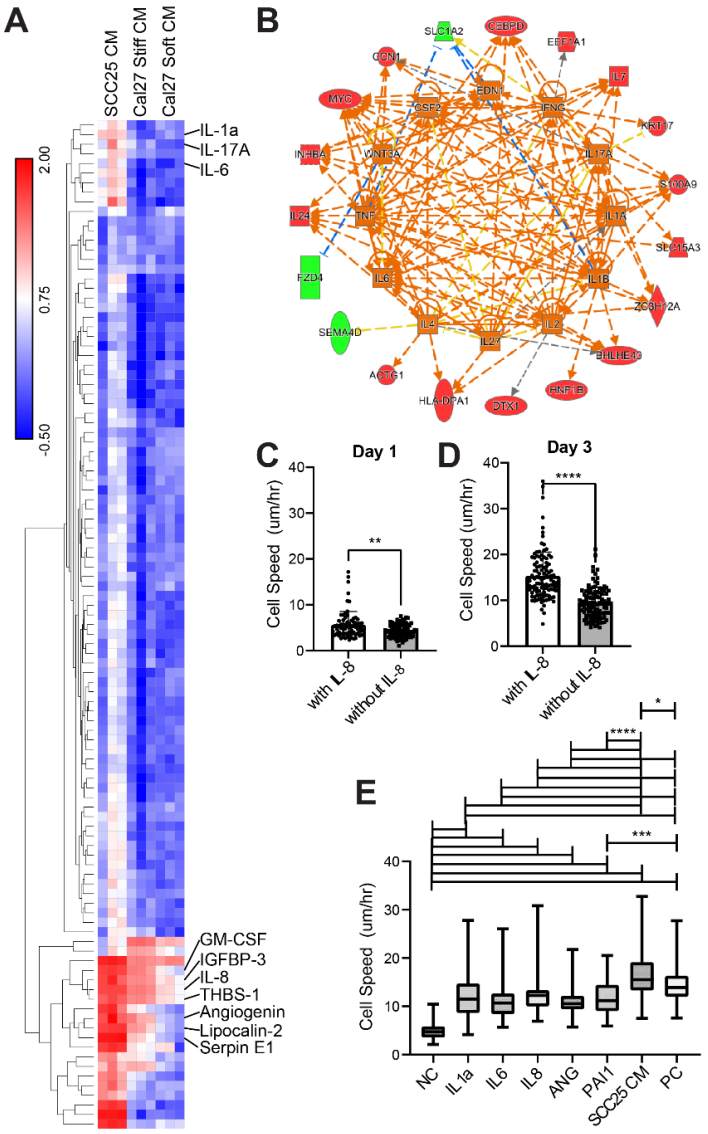


Figure 2.3: Cytokines involved in metastasis-inducing paracrine cell signaling
(A) Heatmap of cytokine array measuring 105 cytokine expression. SCC25-, Cal27 on stiff- and Cal27 on soft-conditioned media's cytokine profile was measured and normalized with fresh growth media. Red and blue indicate up and down-regulation of cytokine relative to fresh growth media. (B) Upstream regulator analysis map from QIAGEN Ingenuity Pathway Analysis (IPA). From up (red) or down (green) regulation of genes from RNA seq result, possible upstream regulators (orange) were extrapolated. Orange and blue arrows indicate predicted activation and inhibition between two components respectively. For those whose findings are inconsistent with the state of downstream molecule, yellow arrow is used. Square refers to cytokine, circle is complex/group, rhombus is enzyme, rectangle is G-protein coupled receptor, horizontal oval is transcriptional regulator, vertical oval is transmembrane receptor, and trapezoid is transporter. Migration velocity of Cal27 cultured with SCC25-CM and IL-8-depleted SCC25-CM was measured on Day 1 (C) and Day 3 (D) of incubation. (E) Fresh SCC25-GM was supplemented with 1 ng/ml of cytokines of either IL-1a, IL-6, IL-8, Angiogenin, or PAI-1 and migration velocity of Cal27 cultured with those media was compared to Cal27 in SCC25-CM or Cal27 on stiff PA gel. *p<0.05, **p<0.01, ***p<0.001, ****p<0.0001 for all data as analyzed by one-way ANOVA with Tukey's multiple comparison test.

Expression of IL-1a, IL-6, IL-8, Angiogenin and Serpin PAI-1 was then used to stratify patients bulk RNA sequencing data from The Cancer Genome Atlas (TCGA). 155 head-neck squamous carcinomas (HNSC) patients whose primary tumor site is either tongue or other and unspecified parts of tongue were computed. The top and bottom quantiles' overall survival (OS) (**Figure 2.4A**) and progression free interval (PFI) (**Figure 2.4B**) showed a trend of difference. The survival rate difference between two groups suggests that upregulation of cytokines could have facilitated tumor metastasis by paracrine cell signaling, and so, profiling those cytokines expression can help predicting the invasiveness of patients tumor.

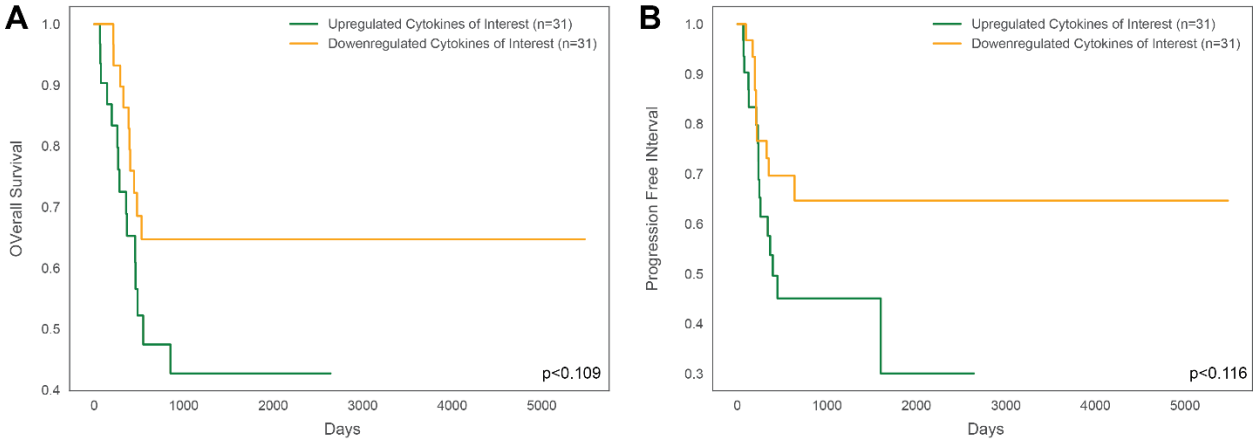


Figure 2.4: Patient survival rate with respect to the transcriptomic expression of the cytokines of interest
Cytokines filtered and tested from Figure 2.3 were used here to stratify patients in The Cancer Genome Atlas (TCGA). Top and bottom quantile of patients in terms of transcriptomic-level cytokine expression had their overall survival (A) and progression free interval (B) compared. The significance of difference between two groups were analyzed with a Log-Rank (Mantel-Cox) test.

2.2.3 MAPK and AKT Signaling Pathways are Activated as Downstream Responses to Paracrine Cell Signaling

Since all 5 cytokines – IL-1a, IL-6, IL-8, Angiogenin, and PAI-1 – enhanced Cal27's migration speed in **Figure 2.3E**, we decided to focus on the intracellular signaling pathways that are commonly related to them. MAPK and AKT signaling pathways are previously studied to be activated by 5 cytokines (Chan et al., 2017/08/08; Guo et al., 2017-12-01; Kubala & Declerck,

2019; Lee et al., 2002/01/01; Mihara et al., 2012/02/01; "Plasminogen Activator Inhibitor 1 Protects Fibrosarcoma Cells from Etoposide-Induced Apoptosis through Activation of the PI3K/Akt Cell Survival Pathway," 2008/10/01; Shen et al., 2017; Trouillon et al., 2011). Western blotting for phosphorylated-ERK1/2 and AKT for Cal27 cultured in SCC25-GM and SCC25-CM demonstrated that Cal27 showed higher activation of both pathways after being exposed to SCC25-CM (**Figure 2.5 A-B**). Involvement of both pathways in the migration enhancing paracrine cell signaling between Cal27 and SCC25 was further supported by pathway inhibition during culturing Cal27 with conditioned media. When 5 uM of Perifosine (AKT inhibitor) and/or 4 nM of SCH772984 (ERK 1/2 inhibitor) were supplemented to SCC25-CM, Cal27's migration speed significantly decreased and was comparable to those in SCC25-GM (**Figure 2.5C**).

To validate inhibition of pathways by the inhibitors, activation of AKT and ERK1/2 was measured after treating Cal27 with inhibitors. The groups with SCH772984 showed lower phosphorylation of ERK 1/2 than those without the inhibitor (**Figure 2.5D-E**). Furthermore, when growth media was supplemented with all 5 cytokines which are thought to be involved in paracrine cell signaling, Cal27's activation of ERK 1/2 has also increased (**Figure 2.5D and F**). Enhanced activation of ERK 1/2 when Cal27 is cultured in either SCC25-CM or cytokine-supplemented growth media and Cal27's no response to conditioned media when their MAPK pathway is interrupted by ERK1/2 inhibition suggest that MAPK pathway is activated during paracrine signaling between SCC25 and Cal27 via IL-1a, IL-6, IL-8, Angiogenin and PAI-1. On the other hand, the groups treated with Perifosine did not show AKT phosphorylation difference in the western blot (**Figure 5D-E**). Besides, supplementation of growth media with cytokines, either individually or altogether, did not bring any difference in the phosphorylation of AKT in Cal27 (**Figure 2.5F**). Comparing AKT phosphorylation in Cal27 cultured with SCC25-CM (**Figure 2.5A**) vs. cytokine supplemented SCC25-GM (**Figure 2.5F**), we can conclude that, though AKT is activated in Cal27 in response to SCC25-CM, it is not in response to the 5

cytokines we identified in the study. Still, treating Cal27 in SCC25-CM with Perifosine discouraged migration enhancement in Cal27. There is a chance that Perifosine affected cell behavior not through AKT pathway inhibition but through other off-target effects. Perifosine is a bioavailable, synthetic anti-cancer alkyl-phospholipid (APL)("Perifosine: update on a novel Akt inhibitor - PubMed," 2009 Mar). Since it is an analogue of phospholipids, building blocks of cellular membrane, Perifosine can interfere lipid-related metabolism, signal transduction, and membrane function (Blitterswijk & Verheij, 2008). Though the most well-known effect of Perifosine is its inhibition of AKT pathway, it can also inhibit other kinases such as protein kinase C (PKC) (Jirousek & Goekjian, 2001-12-1), PDK1 , and even MAPK (Blitterswijk & Verheij, 2008). Since Perifosine functionally interrupted paracrine cell signaling (**Figure 2.5C**), one of the signaling pathways other than AKT that can be inhibited by Perifosine is likely to be involved in the process and should be studied to further understand intra-tumor paracrine cell signaling between heterotypic cell populations in OSCC.

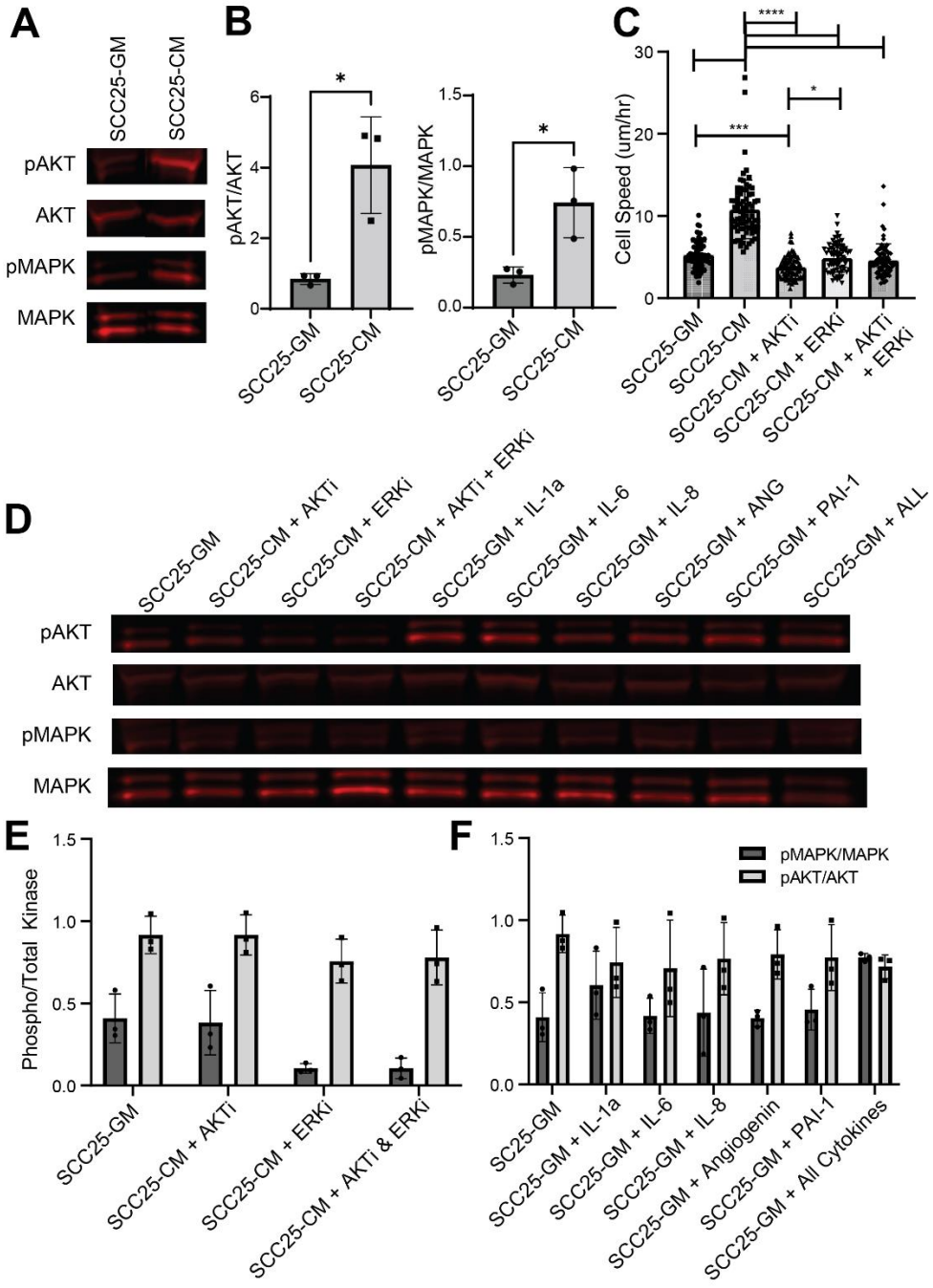


Figure 2.5: MAPK and AKT signaling pathways activated in response to paracrine cell signaling (A) Western blot image of phosphorylated/total AKT and MAPK (ERK1/2) in Cal27 cultured with SCC25-GM vs. SCC25-CM. (B) Quantification of phosphorylated to total kinase expression of AKT (left) and MAPK (right) in Cal27 cultured with SCC25-GM vs. SCC25-CM. (C) SCC25-CM co-cultured Cal27's motility measurement after inhibiting AKT and/or MAPK with inhibitors. *p<0.05, **p<0.01, ***p<0.001, ****p<0.0001 for the data as analyzed by one-way ANOVA with Tukey's multiple comparison test. (D) Western blot image of Cal27 culture with either SCC25-CM with AKT and/or ERK inhibitors or SCC25-GM supplemented with human recombinant cytokines. (E,F) Quantification of western blot result from (D).

2.3 Materials and Methods

Cell Culture and Reagents

OSCC cell lines – Cal27 and SCC25 – were a kind gift from Akihiro Sakai, University of California San Diego (UCSD). Cal27 cells were cultured in DMEM high glucose media (Gibco; 11965-092) supplemented with 10% fetal bovine serum (FBS) (Omega Scientific, FB-01) and 1% penicillin/streptomycin (Gibco, 15140-122). SCC25 cells were cultured in 1:1 DMEM and F12 with HEPES (Gibco; 11330-032) supplemented with 10% FBS, 1% penicillin/streptomycin, and 400 ng/ml of hydrocortisone (Sigma-Aldrich, H0888). For media control group in indirect co-culturing assay, Cal27 was cultured with cell culture media prepared for SCC25 (1:1 DMEM/f12 with 10 % FBS, 1 % penicillin/streptomycin, and 400 ng/ml hydrocortisone) to support that base media difference does not affect cell behavior.

Cells were treated with recombinant human proteins to see how cytokines of our interest functionally affect cells. IL-1a (200-LA-022), IL-6 (206-IL-010), IL-8 (208-IL-010), and Angiogenin (265-AN-050) are from R&D System, and PAI-1 (140-04) from Pepro Tech. Based on titration assay in which cells were treated with 1, 10, and 100 ng/ml of each cytokines, in the time-lapse assay to check the effectiveness of individual cytokines, cells were treated with 1 ng/ml of each recombinant human proteins in 1:1 DMEM/F12 (10 % FBS, 1% penicillin/streptomycin, and 400 ng/ml hydrocortisone).

Polyacrylamide Hydrogels

Glass surface was oxidized by UV/ozone exposure (BioForce Nanosciences) and functionalized with 20 mM 3-(trimethoxysilyl)propyl metharylate (Sigma-Aldrich, #440159) in ethanol. 0.1% (w/v) ammonium persulfate (APS) (Fisher Bioreagents, BP179-25) and 0.1 % (v/v) N,N,N',N'-tetramethylethylenediamine (TEMED) (Fisher Bioreagents, BP150-20) were added to (w/v) 3% acrylamide (Thermo Scientifics, J62480.AP) and 0.06% bis-acrylamide

(Research Products International, 110-26-9) solution in PBS for 0.48 kPa polyacrylamide gel, or 8 % of acrylamide and 0.264 % of bis-acrylamide for 20 kPa. 30 ul of pre-PA solution for 12-well glass bottom tissue culture plate and 40 ul for 25 mm coverslips were sandwiched between methacrylate functionalized glass surface and dichlorodimethylsilane (DCDMS)-treated (Sigma Aldrich, 440272) cover slips or glass slides. After 10 (for 20 kPa PA) or 30 (for 0.48 kPa) minutes of incubation at room temperature, DCDMS-treated cover slips/glass slides were detached. PA gels were incubated with 0.2 mg/ml sulfo-SANPAH (CovaChem, 13414-100) in 50 mM HEPES at 350 nm wavelength UV for 10 min. After 3 times of rinsing with PBS, PA gels were incubated overnight in 0.15 mg/ml collagen type I (Enzo Life Science, ALX-522-435-0100) in PBS at 37 degC. Collagen-coated gels were UV-sterilized for 45 minutes before cells were seeded on them.

Indirect Co-Culture

To prepare SCC25 conditioned media, 0.2*10^6 SCC25 cells per well were seeded on either 6-well plastic tissue culture plate or 0.48 kPa PA gel on 25 mm coverslip with 2 ml of SCC25 culture media per well. After 24-hour incubation at 37 degC and 5% CO2, cell cultured media was replaced and further incubated for 24 hours. Conditioned media was collected and sterile filtered with 0.22 um pore size steriflip (Millipore, SCGP00525). Conditioned media was used to culture naïve Cal27 on 0.48 kPa PA gel right after collection without being stored.

Cal27 from tissue culture plastic flask were trypsizinized and seeded on collagen-coated 0.48 kPa PA gel (every control and experimental groups but positive control) or 20 kPa PA gel (for positive control). After 2 hours of incubation at 37 degC and 5 % CO2, cell culture media was replaced with fresh or conditioned media. The effect of indirect co-culturing was observed for 4 days.

To identify cytokines involved in paracrine cell-cell interaction, 1:1 DMEM/F12 media was supplemented with recombinant human proteins instead of being conditioned by SCC25. Cal27 seeding and incubation process was the same, but 1, 10, 100 ng/ml of IL-1a, IL-6, IL-8, Angiogenin, PAI-1 were added to 1:1 DMEM/F12 fresh media for titration assay. After titration, the concentration of individual cytokines was set to 1 ng/ml.

Time Lapse

After being plated on either 0.48 kPa or 20 kPa PA gels and cultured with appropriate cell culture media for varying duration of time, Cal27 migration was observed with Nikon Eclipse Ti equipped with motorized stage. Image of cells at 10x magnification in brightfield in multiple positions were taken every 15 minutes for 20 hours. During the assay, temperature and CO2 levels were controlled by Live Cell (Pathology Devices, Inc.). 'Manual Tracking' plugin on ImageJ was used to track each cells. The nucleus of each cells was used as a reference point to track.

RNA Sequencing

RNA from Cal27 cells cultured with SCC25-CM for 3 days versus those cultured with fresh DMEM/F12 1:1 media for aday was collected by RNeasy Mini Kit (QIAGEN, 74104). Institute for Genomic Medicine at University of California San Diego processed the extracted RNA. RNA integrity and concentration was analyed by Agilent Tape Station system and Qubit 2.0 Fluorometer, respectively. All submitted samples had RIN numbers above 9.0. RNA library was prepared with Illumina TruSeq Stranded RNA, High Throughput Library Prep Kit, and then sequenced on a NovaSeq 6000. ROSALIND® () analyzed sequenced data with a HyperScale architecture (ROSALIND, San Diego, CA). ROSALIND trimmed the reads with cutadapt, assessed quality score with FastQC, and aligned the reads to human genome build dm6 with STAR. Sample reads were quantified with HTseq. DESeq2 R library normalized the read count

by Relative Log Expression (RLE) and calculated log fold changes and p-values, which is adjusted by optional covariate correction. Clustering of DEGs was visualized on the heatmap generated by Partitioning Around Medoids method using the fpc R library. Functional enrichment analysis of pathways and gene ontology was done by HOMER. Panther was used to assess GO terms for DEGs.

Cytokine Array

Cytokine expression profiles of conditioned media – SCC25-CM, Cal27 stiff-CM, and Cal27 soft -CM – was measured by Proteome Profiler Human XL Cytokine Array Kite (R&D Systems; ARY022B). 0.2*10^6 cells of SCC25 on plastic tissue culture plate, and the same amount of Cal27 were seeded on either stiff (20 kPa) or soft (0.48 kPa) substrate. Cells were incubated with DMEM/F12 1:1 (10% FBS, 1% penicillin/streptomycin, 400 ng/ml hydrocortisone) for 24 hours. After conditioning, media was sterilized with steriflip (Millipore, SCGP00525). To detect cytokines from the samples, cytokine array from R&D system used membrane-based sandwich immunoassay. Nitrocellulose membranes pre-coated with 105 different capture antibodies were incubated with conditioned media at 4 degC overnight on shaker. The membranes were washed 3 times with washing buffer. The cytokines attached to the capture antibody on the membrane were once more detected by biotinylated detection antibodies. The membranes were further treated with streptavidin-horseradish-peroxidase (HRP) conjugate. Membranes were coated with Chemi Reagent Mix from the kit and developed on X-ray film with autoradiography for five minutes. The array results were analyzed by semi-automated analysis of dot blots (Klemm, 2020) with ImageJ.

Ingenuity Pathway Analysis

Upstream regulator analysis was done by QIAGEN ingenuity pathway analysis based on DEGs from RNA sequencing and their lfc and p-value.

Cytokine Depletion

Immunoprecipitation method was used to deplete IL-8 from SCC25-CM. 500ul of SCC25-CM was combined with 10 ug of anti-IL-8 antibody (R&D Systems, MAB208-100) and mixed overnight at 4 degC. 0.25 mg of Pierce Protein A/G Magnetic beads (Thermo Scientifics, PI88802) were washed twice with TBST buffer (0.2% Tween 20). After washing, the conditioned media and antibody mixture was added to the Eppendorf tube with the beads and mixed for an hour at room temperature. The beads were collected with magnetic stand and the flow-through was collected. IL-8-depleted SCC25-CM was sterilized with Steriflip (Millipore, SCGP00525) and used for ELISA or cell culture assay without storage.

ELISA

To quantify the cytokines expression in SCC25-CM, and Cal27 on soft-CM, sandwich ELISA was used. ELISA for IL-8 exceptionally had 3 samples including IL-8 eliminated version of SCC25-CM with immunoprecipitation. ELISA kit used for each target is like following: Angiogenin (abcam, ab219629), GM-CSF (BioLegend, 432004), IGFBP-3 (Invitrogen, EHIGFBP3), IL-1a (abcam, ab178008), IL-17A (abcam, ab216167), IL-6 (abcam, ab178013), IL-8 (BioLegend, 431504), Lipocalin-2 (abcam, ab215541), PAI-1 (abcam, ab269373), Thrombospondin-1 (Invitrogen, EHTHBS1). Instruction for each kit was followed. Standard of each ELISA run was prepared with diluent in the kit. Microplates were coated with capture antibody (overnight), blocking buffer (1 hour), diluted samples (2 hours), and detection antibody (1 hour) in order (BioLegend and Invitrogen) or all of them (1 hour) together (abcam) at room temperature on plate shaker. In between every step, the plates were washed 3 times with washing buffer. The detection antibodies are conjugated with biotins. The plates were incubated with Streptavidin-HRP solution (30-45 min) and then TMB substrate (5-15 min) at room temperature on shaker. The reaction of HRP and TMB substrate was stopped with stop solution.

The plates optical density (OD, 450 nm) with reference OD at 570 nm were read with Envision plate reader using Tecan software.

Western Blot

Cal27 was seeded on soft PA gel with Cal27-GM and incubated for 2 hours. After incubation, the media was replaced with either SCC25-GM, SCC25-GM supplemented with cytokine, or SCC25-CM and incubated 30 min further. The cells were lysed with mRIPA buffer and the amount of protein in cell lysates were quantified with BCA assay kit (Thermo Scientifics, 23225). 10ug of protein per sample was denatured by 4x Laemmli buffer (BioRad, 1610747), 50mM DTT, and mRIPA. Denatured samples were deactivated at 95 degC for 5 min. The samples were loaded to 4-12 % Bis-Tris gel (Thermo Fisher Scientific, NW04122BOX), and the gel underwent electrophoresis under 70 V. The gel was blotted on nitrocellulose membrane with iBlot semi-dry transfer system (Invitrogen, IB301001). The membrane was blocked with Azure Fluorescent Blot Blocking Buffer (Azure Biosystems, AC2190) with 1% bovine serum albumin (BSA) on shaker at room temperature. After blocking, the membrane was incubated with primary antibody – ERK 1/2 (1:1000, Cell Signaling Technology, #4695), phospho-ERK 1/2 (1:1000, Cell Signaling Technology, #9101), AKT (1:1000, Cell Signaling Technology, #9272), and phospho-AKT (1:1000, Cell Signaling Technology, #4060) – overnight at 4 degC, and then with donkey anti-rabbit IgG secondary antibody (1:2000, 680nm, Invitrogen, A10043) at room temperature for 1 hour on shaker. In between the steps of antibody coating and before imaging, the membrane was washed (3X) with TBST buffer for 5 min on shaker. The image was developed with LI-COR Odyssey CLx imaging software and analyzed by Image Studio Lite. The amount of phosphorylated proteins were normalized by the expression of total amount of the protein.

KM Plot

Bulk RNA sequencing data of head-neck squamous carcinoma (HNSC) patients from The Cancer Genome Atlas (TCGA) were downloaded from NIH NCI GDC Data portal. The primary tumor sites of the patients data specifically used for this study were either tongue or other and unspecified parts of tongue. Corresponding clinical metadata were obtained from {Liu, 2018}. To correlate 5-year survival rate of patients with transcriptomic upregulation of cytokines that are likely to be involved in paracrine cell-cell metastasis-inducing communication, we normalized the expression of each gene per patient with z-score based on the mean of the gene's expression across the whole patient data. Per patient, normalized z-score of 5 cytokine genes were summed. Z-score based quantiles were mapped on KM plot to "Cytokines Up-regulated" vs. "Cytokines Down-regulated" groups. Overall survival (OS) and progression free interval (PFI) comparing top and bottom quantiles were plotted with Kaplan-Meier method. Log-rank test was used to determine the significance of the survival rate difference between two groups. Lifelines python library is included in the patient survival rate analysis.

Statistics

All data is shown from triplicate biological replicates. For 2D migration assays, data was analyzed by one-way ANOVA with Tukey's post-test or multiple comparisons test as indicated. For all analyses, *$p<0.05$, **$p<0.01$, ***$p<0.001$, ****$p<0.0001$. Significance for TCGA analyses were performed with a Log-Rank (Mantel-Cox) test. Data expressed as box-and-whisker plots show all points with the mean and whisker ends corresponding to minimum and maximum values. All other values are expressed as mean +/- standard deviation. Statistical analyses were performed using Prism software.

Acknowledgements

Chapter 2, in full, is currently being prepared for submission for publication of the

material. Moon, So Youn; Lamers, Marcelo L.; Engler Adam J. The dissertation author was the primary investigator and author of this material.

REFERENCES

Aguilar-Cuenca, R., Juanes-García, A., & Vicente-Manzanares, M. (2014). Myosin II in mechanotransduction: master and commander of cell migration, morphogenesis, and cancer. In *Cellular and molecular life sciences : CMLS* (Vol. 71, pp. 479-492): Cell Mol Life Sci.

Alamoud, K. A., Kukuruzinska, M. A., & K.A. Alamoud, M. A. K. (2018-05-17). Emerging Insights into Wnt/β-catenin Signaling in Head and Neck Cancer. *Journal of Dental Research*, *97*(6). https://doi.org/10.1177/0022034518771923

Alonso-Nocelo, M., Raimondo, T. M., Vining, K. H., López-López, R., De La Fuente, M., & Mooney, D. J. (2018). Matrix stiffness and tumor-associated macrophages modulate epithelial to mesenchymal transition of human adenocarcinoma cells. In.

Alves, A., Diel, L., Ramos, G., Pinto, A., Bernardi, L., Yates, J., & Lamers, M. (2021). Tumor microenvironment and Oral Squamous Cell Carcinoma: A crosstalk between the inflammatory state and tumor cell migration. In *Oral Oncology* (Vol. 112, pp. 105038): Pergamon.

Baker, A. M., Bird, D., Lang, G., Cox, T. R., & Erler, J. T. (2013). Lysyl oxidase enzymatic function increases stiffness to drive colorectal cancer progression through FAK. In *Oncogene* (Vol. 32, pp. 1863-1868): Oncogene.

Banisadr, A., Eick, M., Beri, P., Parisian, A. D., Yeoman, B., Placone, J. K.,…Furnari, F. (2020). EGFRvIII uses intrinsic and extrinsic mechanisms to reduce glioma adhesion and increase migration. In.

Beri, P., Popravko, A., Yeoman, B., Kumar, A., Chen, K., Hodzic, E., Chiang, A., Banisadr, A., Placone, J. K., Carter, H., Fraley, S. I., Katira, P., & Engler, A. J. (2020). Cell adhesiveness serves as a biophysical marker for metastatic potential. In *Cancer Research* (Vol. 80, pp. 901-911): American Association for Cancer Research Inc.

Blitterswijk, W. J. v., & Verheij, M. (2008). Anticancer Alkylphospholipids: Mechanisms of Action, Cellular Sensitivity and Resistance, and Clinical Prospects. *Current Pharmaceutical Design*, *14*(21). https://doi.org/10.2174/138161208785294636

Bonnans, C., Chou, J., & Werb, Z. (2014). Remodelling the extracellular matrix in development and disease. In *Nature reviews. Molecular cell biology* (Vol. 15, pp. 786-801): Nat Rev Mol Cell Biol.

Boudreau, A., Van't Veer, L. J., & Bissell, M. J. (2012). An "elite hacker": breast tumors exploit the normal microenvironment program to instruct their progression and biological diversity. In *Cell adhesion & migration* (Vol. 6, pp. 236-435): Cell Adh Migr.

Burgstaller, G., Oehrle, B., Gerckens, M., White, E. S., Schiller, H. B., & Eickelberg, O. (2017). The instructive extracellular matrix of the lung: basic composition and alterations in chronic lung disease. In *The European respiratory journal* (Vol. 50): Eur Respir J.

Butcher, D. T., Alliston, T., & Weaver, V. M. (2009). A tense situation: forcing tumour progression. In *Nature reviews. Cancer* (Vol. 9, pp. 108-122): Nat Rev Cancer.

Calvo, F., Ege, N., Grande-Garcia, A., Hooper, S., Jenkins, R. P., Chaudhry, S. I.,Harrington, K., Williamson, P., Moeendarbary, E., Charras, G., & Sahai, E. (2013). Mechanotransduction and YAP-dependent matrix remodelling is required for the generation and maintenance of cancer-associated fibroblasts. In *Nature cell biology* (Vol. 15, pp. 637-646): Nat Cell Biol.

Carey, S. P., Starchenko, A., McGregor, A. L., & Reinhart-King, C. A. (2013). Leading malignant cells initiate collective epithelial cell invasion in a three-dimensional heterotypic tumor spheroid model. In *Clinical and Experimental Metastasis* (Vol. 30, pp. 615-630): Springer.

Chan, L.-P., Liu, C., Chiang, F.-Y., Wang, L.-F., Lee, K.-W., Chen, W.-T.,Kuo, P.-L., & Liang, C.-H. (2017/08/08). IL-8 promotes inflammatory mediators and stimulates activation of p38 MAPK/ERK-NF-κB pathway and reduction of JNK in HNSCC. *Oncotarget*, *8*(34). https://doi.org/10.18632/oncotarget.16914

Chaudhuri, O., Koshy, S. T., Branco Da Cunha, C., Shin, J. W., Verbeke, C. S., Allison, K. H., & Mooney, D. J. (2014). Extracellular matrix stiffness and composition jointly regulate the induction of malignant phenotypes in mammary epithelium. In *Nature materials* (Vol. 13, pp. 970-978): Nat Mater.

Chen, Y., Terajima, M., Yang, Y., Sun, L., Ahn, Y. H., Pankova, D.,Puperi, D. S., Watanabe, T., Kim, M. P., Blackmon, S. H., Rodriguez, J., Liu, H., Behrens, C., Wistuba, I. I., Minelli, R. Scott, K. L., Sanchez-Adams, J., Guilak, F., Pati, D., Thilaganathan, N., Burns, A. R., Creighton, C. J., Martinez, E. D., Zal, T., Grande-Allen, K. J., Yamuchi, M., & Kurie, J. M. (2015). Lysyl hydroxylase 2 induces a collagen cross-link switch in tumor stroma. In *The Journal of clinical investigation* (Vol. 125, pp. 1147-1162): J Clin Invest.

Chen, Y. W., Kao, S. Y., Wang, H. J., & Yang, M. H. (2013). Histone modification patterns correlate with patient outcome in oral squamous cell carcinoma. In *Cancer* (Vol. 119, pp. 4259-4267): Cancer.

Chi, A. C., Day, T. A., & Neville, B. W. (2015). Oral cavity and oropharyngeal squamous cell carcinoma--an update. In *CA: a cancer journal for clinicians* (Vol. 65, pp. 401-421): CA Cancer J Clin.

Chin, L. K., Xia, Y., Discher, D. E., & Janmey, P. A. (2016). Mechanotransduction in cancer. In *Current opinion in chemical engineering* (Vol. 11, pp. 77-84): Curr Opin Chem Eng.

Dias, K. B., Flores, A. P. C., Hildebrand, L. D. C., De Oliveira, M. G., Lamers, M. L., Rados, P. V., Magnusson, A. S., & Filho, M. S. A. (2019). Non-muscle myosin II as a predictive factor in head and neck squamous cell carcinoma. In *Medicina oral, patologia oral y cirugia bucal* (Vol. 24, pp. e346-e353): Med Oral Patol Oral Cir Bucal.

Erdogan, B., Ao, M., White, L. M., Means, A. L., Brewer, B. M., Yang, L., Washington, M. K.,

Shi, C., Franco, O. E., Weaver, A. M., Hayward, S. W., Li, D., & Webb, D. J. (2017). Cancer-associated fibroblasts promote directional cancer cell migration by aligning fibronectin. In *The Journal of cell biology* (Vol. 216, pp. 3799-3816): J Cell Biol.

Fattet, L., Jung, H. Y., Matsumoto, M. W., Aubol, B. E., Kumar, A., Adams, J. A., Chen, A. C., Sah, R. L., Engler, A. J., Pasquale, E. B., & Yang, J. (2020). Matrix Rigidity Controls Epithelial-Mesenchymal Plasticity and Tumor Metastasis via a Mechanoresponsive EPHA2/LYN Complex. In *Developmental cell* (Vol. 54, pp. 302-316.e307): Dev Cell.

Frantz, C., Stewart, K. M., & Weaver, V. M. (2010). The extracellular matrix at a glance. In *Journal of cell science* (Vol. 123, pp. 4195-4200): J Cell Sci.

Friedl, P., Locker, J., Sahai, E., & Segall, J. E. (2012). Classifying collective cancer cell invasion. In *Nature cell biology* (Vol. 14, pp. 777-783): Nat Cell Biol.

Fujii, S., Tajiri, Y., Hasegawa, K., Matsumoto, S., Yoshimoto, R. U., Wada, H., Kishida, S., Kido, M. A., Yoshikawa, H., Ozeki, S., & Kiyoshima, T. (2020). The TRPV4-AKT axis promotes oral squamous cell carcinoma cell proliferation via CaMKII activation. In *Laboratory investigation; a journal of technical methods and pathology* (Vol. 100, pp. 311-323): Lab Invest.

Geiger, B., Bershadsky, A., Pankov, R., & Yamada, K. M. (2001). Transmembrane crosstalk between the extracellular matrix--cytoskeleton crosstalk. In *Nature reviews. Molecular cell biology* (Vol. 2, pp. 793-805): Nat Rev Mol Cell Biol.

Guo, Y., Zang, Y., Lv, L., Cai, F., Qian, T., Zhang, G., & Feng, Q. (2017-12-01). IL-8 promotes proliferation and inhibition of apoptosis via STAT3/AKT/NF-κB pathway in prostate cancer Corrigendum in /10.3892/mmr.2019.9942. *Molecular Medicine Reports*, *16*(6). https://doi.org/10.3892/mmr.2017.7747

Hanahan, D., & Weinberg, R. A. (2011). Hallmarks of cancer: the next generation. In *Cell* (Vol. 144, pp. 646-674): Cell.

Hoelzinger, D. B., Demuth, T., & Berens, M. E. (2007/11/07). Autocrine Factors That Sustain Glioma Invasion and Paracrine Biology in the Brain Microenvironment. *JNCI: Journal of the National Cancer Institute*, *99*(21). https://doi.org/10.1093/jnci/djm187

Huang, S., & Ingber, D. E. (2005). Cell tension, matrix mechanics, and cancer development. In *Cancer Cell* (Vol. 8, pp. 175-176): Cell Press.

Jensen, J. S., Jakobsen, K. K., Mirian, C., Christensen, J. T., Schneider, K., Nahavandipour, A.,…Buchwald, C. v. (2019). The Copenhagen Oral Cavity Squamous Cell Carcinoma database: protocol and report on establishing a comprehensive oral cavity cancer database. In *Clinical epidemiology* (Vol. 11, pp. 733-741): Clin Epidemiol.

Jing, Y., Han, Z., Zhang, S., Liu, Y., & Wei, L. (2011). Epithelial-Mesenchymal Transition in tumor microenvironment. *Cell & Bioscience*, *1*(1). https://doi.org/10.1186/2045-3701-1-29

Jirousek, M. R., & Goekjian, P. G. (2001-12-1). Protein kinase C inhibitors as novel anticancer drugs. *Expert Opinion on Investigational Drugs*, *10*(12). https://doi.org/10.1517/13543784.10.12.2117

Johnson, N. W., Jayasekara, P., Amarasinghe, A. A., & Hemantha, K. (2011). Squamous cell carcinoma and precursor lesions of the oral cavity: epidemiology and aetiology. In *Periodontology 2000* (Vol. 57, pp. 19-37): Periodontol 2000.

Kamangar, F., Dores, G. M., & Anderson, W. F. (2006). Patterns of cancer incidence, mortality, and prevalence across five continents: defining priorities to reduce cancer disparities in different geographic regions of the world. In *Journal of clinical oncology : official journal of the American Society of Clinical Oncology* (Vol. 24, pp. 2137-2150): J Clin Oncol.

Koontongkaew, S. (2013). The Tumor Microenvironment Contribution to Development, Growth, Invasion and Metastasis of Head and Neck Squamous Cell Carcinomas. *Journal of Cancer*, *4*(1). https://doi.org/10.7150/jca.5112

Kraning-Rush, C. M., & Reinhart-King, C. A. (2012-5-1). Controlling matrix stiffness and topography for the study of tumor cell migration. *Cell Adhesion & Migration*, *6*(3). https://doi.org/10.4161/cam.21076

Kubala, M. H., & Declerck, Y. A. (2019). The plasminogen activator inhibitor-1 paradox in cancer: a mechanistic understanding. *Cancer and Metastasis Reviews*, *38*(3), 483-492. https://doi.org/10.1007/s10555-019-09806-4

Lauffenburger, D. A., & Horwitz, A. F. (1996). Cell migration: a physically integrated molecular process. In *Cell* (Vol. 84, pp. 359-369): Cell.

Lee, W. H., Choong, L. Y., Jin, T. H., Mon, N. N., Chong, S., Liew, C. S., Putti, T., LU, S. Y., Harteneck, C., & Lim, Y. P. (2017). TRPV4 plays a role in breast cancer cell migration via Ca 2+-dependent activation of AKT and downregulation of E-cadherin cell cortex protein. In *Oncogenesis* (Vol. 6, pp. e338-e338): Oncogenesis.

Lee, Z. H., Lee, S. E., Kim, C.-W., Lee, S. H., Kim, S. W., Kwack, K., Walsh, K., & Kim, H.-H. (2002/01/01). IL-1α Stimulation of Osteoclast Survival through the PI 3-Kinase/Akt and ERK Pathways1. *The Journal of Biochemistry*, *131*(1). https://doi.org/10.1093/oxfordjournals.jbchem.a003071

Levental, K. R., Yu, H., Kass, L., Lakins, J. N., Egeblad, M., Erler, J. T., Fong, S. F. T., Csiszar, K., Giaccia, A., Weninger, W., Yamauchi, M., Gasser, D. L., & Weaver, V. M. (2009). Matrix crosslinking forces tumor progression by enhancing integrin signaling. In *Cell* (Vol. 139, pp. 891-906): Cell.

Liu, J., Lichtenberg, T., Hoadley, K. A., Poisson, L. M., Lazar, A. J., Cherniack, A. D.,…Hu, H. (2018). An Integrated TCGA Pan-Cancer Clinical Data Resource to Drive High-Quality Survival Outcome Analytics. In *Cell* (Vol. 173, pp. 400-416.e411): Cell Press.

Lu, P., Weaver, V. M., & Werb, Z. (2012). The extracellular matrix: a dynamic niche in cancer progression. In *The Journal of cell biology* (Vol. 196, pp. 395-406): J Cell Biol.

Matrix stiffness mechanically conditions EMT and migratory behavior of oral squamous cell carcinoma, 132 Company of Biologists Ltd (2019).

Melzer, C., Yang, Y., Hass, R., Melzer, C., Yang, Y., & Hass, R. (2016-09-08). Interaction of MSC with tumor cells. *Cell Communication and Signaling 2016 14:1*, *14*(1). https://doi.org/10.1186/s12964-016-0143-0

Mihara, M., Hashizume, M., Yoshida, H., Suzuki, M., & Shiina, M. (2012/02/01). IL-6/IL-6 receptor system and its role in physiological and pathological conditions. *Clinical Science*, *122*(4). https://doi.org/10.1042/CS20110340

Mitra, S. K., Hanson, D. A., & Schlaepfer, D. D. (2005). Focal adhesion kinase: in command and control of cell motility. In *Nature reviews. Molecular cell biology* (Vol. 6, pp. 56-68): Nat Rev Mol Cell Biol.

Mitra, S. K., & Schlaepfer, D. D. (2006). Integrin-regulated FAK-Src signaling in normal and cancer cells. In *Current opinion in cell biology* (Vol. 18, pp. 516-523): Curr Opin Cell Biol.

Montero, P. H., & Patel, S. G. (2015). Cancer of the oral cavity. In *Surgical oncology clinics of North America* (Vol. 24, pp. 491-508): Surg Oncol Clin N Am.

Moon, S. Y., De Campos, P. S., Matte, B. F., Placone, J. K., Zanella, V. L. G., Martins, M. D.,…Engler, A. J. (2023). Cell contractility drives mechanical memory of oral squamous cell carcinoma. *Molecular Biology of the Cell*, *34*(9). https://doi.org/10.1091/mbc.e22-07-0266

Nasrollahi, S., Walter, C., Loza, A. J., Schimizzi, G. V., Longmore, G. D., & Pathak, A. (2017). Past matrix stiffness primes epithelial cells and regulates their future collective migration through a mechanical memory. In *Biomaterials* (Vol. 146, pp. 146-155): Biomaterials.

Newell-Litwa, K. A., Horwitz, R., & Lamers, M. L. (2015). Non-muscle myosin II in disease: mechanisms and therapeutic opportunities. In *Disease models & mechanisms* (Vol. 8, pp. 1495-1515): Dis Model Mech.

Ondeck, M. G., Kumar, A., Placone, J. K., Plunkett, C. M., Matte, B. F., Wong, K. C., Fattet, L., Yang, J., & Engler, A. J. (2019). Dynamically stiffened matrix promotes malignant transformation of mammary epithelial cells via collective mechanical signaling. In *Proceedings of the National Academy of Sciences of the United States of America* (Vol. 116, pp. 3502-3507): National Academy of Sciences.

Parsons, J. T., Horwitz, A. R., & Schwartz, M. A. (2010). Cell adhesion: integrating cytoskeletal dynamics and cellular tension. In *Nature reviews. Molecular cell biology* (Vol. 11, pp. 633-643): Nat Rev Mol Cell Biol.

Paszek, M. J., Zahir, N., Johnson, K. R., Lakins, J. N., Rozenberg, G. I., Gefen, A.,…Weaver, V. M. (2005). Tensional homeostasis and the malignant phenotype. In *Cancer cell* (Vol. 8, pp. 241-254): Cancer Cell.

Peglion, F., Llense, F., & Etienne-Manneville, S. (2014). Adherens junction treadmilling during collective migration. In *Nature cell biology* (Vol. 16, pp. 639-651): Nat Cell Biol.

Perifosine: update on a novel Akt inhibitor - PubMed. (2009 Mar). *Current oncology reports*, *11*(2). https://doi.org/10.1007/s11912-009-0016-4

Pickup, M. W., Mouw, J. K., & Weaver, V. M. (2014). The extracellular matrix modulates the hallmarks of cancer. In *EMBO reports* (Vol. 15, pp. 1243-1253): EMBO Rep.

Pires, F. R., Ramos, A. B., de Oliveira, J. B. C., Tavares, A. S., de Luz, P. S. R., & dos Santos, T. C. R. B. (2013). Oral squamous cell carcinoma: clinicopathological features from 346

cases from a single oral pathology service during an 8-year period. In *Journal of applied oral science : revista FOB* (Vol. 21, pp. 460-467): J Appl Oral Sci.

Plasminogen Activator Inhibitor 1 Protects Fibrosarcoma Cells from Etoposide-Induced Apoptosis through Activation of the PI3K/Akt Cell Survival Pathway. (2008/10/01). *Neoplasia*, *10*(10). https://doi.org/10.1593/neo.08486

Ridley, A. J., Schwartz, M. A., Burridge, K., Firtel, R. A., Ginsberg, M. H., Borisy, G.,Parsons, J. T., & Horwitz, A. R. (2003). Cell migration: integrating signals from front to back. In *Science (New York, N.Y.)* (Vol. 302, pp. 1704-1709): Science.

Rogenhofer, S., Miersch, H., Göke, F., Kahl, P., Wieland, W. F., Hofstädter, F., Kristiansen, G., Von Ruecker, A., Muller, S. C., & Ellinger, J. (2013). Histone methylation defines an epigenetic entity in penile squamous cell carcinoma. In *Journal of Urology* (Vol. 189, pp. 1117-1122).

Sawada, K., Morishige, K. i., Tahara, M., Ikebuchi, Y., Kawagishi, R., Tasaka, K., & Murata, Y. (2002). Lysophosphatidic acid induces focal adhesion assembly through Rho/Rho-associated kinase pathway in human ovarian cancer cells. In *Gynecologic oncology* (Vol. 87, pp. 252-259): Gynecol Oncol.

Scully, C., & Bagan, J. (2009). Oral squamous cell carcinoma overview. In *Oral oncology* (Vol. 45, pp. 301-308): Oral Oncol.

Seong, J., Wang, N., & Wang, Y. (2013). Mechanotransduction at focal adhesions: from physiology to cancer development. In *Journal of cellular and molecular medicine* (Vol. 17, pp. 597-604): J Cell Mol Med.

Sharma, S., Goswami, R., Zhang, D. X., & Rahaman, S. O. (2019). TRPV4 regulates matrix stiffness and TGFβ1-induced epithelial-mesenchymal transition. In *Journal of cellular and molecular medicine* (Vol. 23, pp. 761-774): J Cell Mol Med.

Shen, T. N.-Y., Kanazawa, S., Kado, M., Okada, K., Luo, L., Hayashi, A., Mizuno, H., Tanaka, R. (2017). Interleukin-6 stimulates Akt and p38 MAPK phosphorylation and fibroblast migration in non-diabetic but not diabetic mice. *PLoS ONE*, *12*(5). https://doi.org/10.1371/journal.pone.0178232

Stowers, R. S., Shcherbina, A., Israeli, J., Gruber, J. J., Chang, J., Nam, S., Ralbiee, A., Teruel, M. N., Snyder, M. P., Kundaje, A., & Chaudhuri, O. (2019). Matrix stiffness induces a tumorigenic phenotype in mammary epithelium through changes in chromatin accessibility. In *Nature biomedical engineering* (Vol. 3, pp. 1009-1019): Nat Biomed Eng.

Sunami, Y., Häußler, J., Zourelidis, A., Kleeff, J., Sunami, Y., Häußler, J., Zourelidis, A., & Kleeff, J. (2022-01-31). Cancer-Associated Fibroblasts and Tumor Cells in Pancreatic Cancer Microenvironment and Metastasis: Paracrine Regulators, Reciprocation and Exosomes. *Cancers 2022, Vol. 14, Page 744*, *14*(3). https://doi.org/10.3390/cancers14030744

Tilghman, R. W., Cowan, C. R., Mih, J. D., Koryakina, Y., Gioeli, D., Slack-Davis, J. K., Blackman, B.R., Tschumperlin, D. J., & Parsons, J. T. (2010). Matrix rigidity regulates cancer cell growth and cellular phenotype. In *PloS one* (Vol. 5): PLoS One.

Trouillon, R., O'Hare, D., & Chang, S.-I. (2011). An electrochemical functional assay for the sensing of nitric oxide release induced by angiogenic factors. *BMB Reports*, *44*(11), 699-704. https://doi.org/10.5483/bmbrep.2011.44.11.699

Umesh, V., Rape, A. D., Ulrich, T. A., & Kumar, S. (2014). Microenvironmental stiffness enhances glioma cell proliferation by stimulating epidermal growth factor receptor signaling. In *PloS one* (Vol. 9): PLoS One.

Van Helvert, S., Storm, C., & Friedl, P. (2018). Mechanoreciprocity in cell migration. In *Nature cell biology* (Vol. 20, pp. 8-20): Nat Cell Biol.

Vasudevan, J., Lim, C. T., & Fernandez, J. G. (2020/12/01). Cell Migration and Breast Cancer Metastasis in Biomimetic Extracellular Matrices with Independently Tunable Stiffness. *Advanced Functional Materials*, *30*(49). https://doi.org/10.1002/adfm.202005383

Vicente-Manzanares, M., Koach, M. A., Whitmore, L., Lamers, M. L., & Horwitz, A. F. (2008). Segregation and activation of myosin IIB creates a rear in migrating cells. In *The Journal of cell biology* (Vol. 183, pp. 543-554): J Cell Biol.

Wang, N., Tytell, J. D., & Ingber, D. E. (2009). Mechanotransduction at a distance: mechanically coupling the extracellular matrix with the nucleus. In *Nature reviews. Molecular cell biology* (Vol. 10, pp. 75-82): Nat Rev Mol Cell Biol.

Wang, Q., Liu, M., Kozasa, T., Rothstein, J. D., Sternweis, P. C., & Neubig, R. R. (2004). Thrombin and lysophosphatidic acid receptors utilize distinct rhoGEFs in prostate cancer cells. In *The Journal of biological chemistry* (Vol. 279, pp. 28831-28834): J Biol Chem.

Warnakulasuriya, S. (2009). Global epidemiology of oral and oropharyngeal cancer. In *Oral oncology* (Vol. 45, pp. 309-316): Oral Oncol.

Webber, L. P., Wagner, V. P., Curra, M., Vargas, P. A., Meurer, L., Carrard, V. C., Squarize, C. H., Castilho, R. M., & Martins, M. D. (2017). Hypoacetylation of acetyl-histone H3 (H3K9ac) as marker of poor prognosis in oral cancer. In *Histopathology* (Vol. 71, pp. 278-286): Blackwell Publishing Ltd.

Wei, S. C., Fattet, L., Tsai, J. H., Guo, Y., Pai, V. H., Majeski, H. E., Chen, A. C., Sah, R. L., Taylor, S. S., Engler, A. J., & Yang, J. (2015). Matrix stiffness drives epithelial-mesenchymal transition and tumour metastasis through a TWIST1-G3BP2 mechanotransduction pathway. In *Nature cell biology* (Vol. 17, pp. 678-688): Nat Cell Biol.

Wei, X., Lou, H., Zhou, D., Jia, Y., Li, H., Huang, Q., Ma, J., Yang, Z., Sun, C., Meng, Y., Xu, S., Yang, X., Li, X., Ji, T., Guo, Z., & Gao, Q. (2021). TAGLN mediated stiffness-regulated ovarian cancer progression via RhoA/ROCK pathway. In *Journal of experimental & clinical cancer research : CR* (Vol. 40): J Exp Clin Cancer Res.

Wong, S. Y., Ulrich, T. A., Deleyrolle, L. P., MacKay, J. L., Lin, J. M. G., Martuscello, R. T., Jundi, M. A., Reynolds, B. A., & Kumar, S. (2015). Constitutive activation of myosin-dependent contractility sensitizes glioma tumor-initiating cells to mechanical inputs and reduces tissue invasion. In *Cancer research* (Vol. 75, pp. 1113-1122): Cancer Res.

Wozniak, M. A., & Chen, C. S. (2009). Mechanotransduction in development: a growing role for

contractility. In *Nature reviews. Molecular cell biology* (Vol. 10, pp. 34-43): Nat Rev Mol Cell Biol.

Wu, Y. I., Frey, D., Lungu, O. I., Jaehrig, A., Schlichting, I., Kuhlman, B., & Hahn, K. M. (2009). A genetically encoded photoactivatable Rac controls the motility of living cells. In *Nature* (Vol. 461, pp. 104-108): Nature.

Yamada, K. M., & Sixt, M. (2019). Mechanisms of 3D cell migration. In *Nature reviews. Molecular cell biology* (Vol. 20, pp. 738-752): Nat Rev Mol Cell Biol.

Yeoman, B., Shatkin, G., Beri, P., Banisadr, A., Katira, P., & Engler, A. J. (2021). Adhesion strength and contractility enable metastatic cells to become adurotactic. In *Cell reports* (Vol. 34): Cell Rep.

Yu, M., Shen, W., Shi, X., Wang, Q., Zhu, L., Xu, X., Yu, J., & Liu, L. (2019). Upregulated LOX and increased collagen content associated with aggressive clinicopathological features and unfavorable outcome in oral squamous cell carcinoma. In *Journal of cellular biochemistry* (Vol. 120, pp. 14348-14359): J Cell Biochem.

Zhang, B., Gao, S., Li, R., Li, Y., Cao, R., Cheng, J., Guo, Y., Wang, E., Huang, Y. & Zhang, K. (2020). Tissue mechanics and expression of TROP2 in oral squamous cell carcinoma with varying differentiation. In *BMC cancer* (Vol. 20): BMC Cancer.

Zhang, J. Y., Zhu, W. W., Wang, M. Y., Zhai, R. D., Wang, Q., Shen, W. L., & Liu, L. K. (2021). Cancer-associated fibroblasts promote oral squamous cell carcinoma progression through LOX-mediated matrix stiffness. In *Journal of translational medicine* (Vol. 19): J Transl Med.